Silicon Compound Nanomaterials: Exploring Emission Mechanisms and Photobiological Applications

Dutt, Ateet; Salinas, Rafael Antonio; Martínez-Tolibia, Shirlley E.; Ramos-Serrano, Juan Ramón; Jain, Manmohan; Hamui, Leon; Ramos, Carlos David; Mostafavi, Ebrahim; Kumar Mishra, Yogendra; Matsumoto, Yasuhiro; Santana, Guillermo; Thakur, Vijay Kumar; Kaushik, Ajeet Kumar

Link to publication

REVIEW

**ADVANCED
PHOTONICS
RESEARCH**
Open Access

www.adpr-journal.com

Silicon Compound Nanomaterials: Exploring Emission Mechanisms and Photobiological Applications

Ateet Dutt,* Rafael Antonio Salinas, Shirlley E. Martínez-Tolibia, Juan Ramón Ramos-Serrano, Manmohan Jain, Leon Hamui, Carlos David Ramos, Ebrahim Mostafavi, Yogendra Kumar Mishra, Yasuhiro Matsumoto, Guillermo Santana, Vijay Kumar Thakur, and Ajeet Kumar Kaushik

After the first visible photoluminescence (PL) from porous silicon (pSi), continuous efforts are made to fabricate Si-based compound nanomaterials embedded in matrices such as oxide, nitride, and carbide to improve optical performance and industrial acceptability. These nanomaterials' functional and desired properties (nanoparticles and quantum dots embedded in matrices) can vary significantly when embedded in technologically relevant matrices. However, exploring the exact emission mechanisms is one of the remaining challenges from the past few decades. To cover this gap, this review discusses the morphological and optoelectronic properties of Si-based compound nanomaterials and their correlation with the quantum confinement effect and different surface states to find precise emission mechanisms. One of the biggest challenges of using silicon nanomaterials in the biological sector is the development of sensitive materials of low/acceptable toxicity for identifying target analytes either inside/outside the biological platforms. In this scenario, silicon-based compound matrices can offer different characteristics and advantages depending on their size configurations and PL emission mechanisms. On the other hand, a proper understanding of these multifaceted silicon nanomaterials' optical properties (emission mechanisms) can be exploited for pathogen detection and in situ applications in cells and tissues, embarking on a new era of bioimaging technology.

1. Introduction

The linkage between multiple fields of knowledge is one aspect to consider for generating high-impact developments. In that direction, nanotechnology is an emerging field that uses the information and expertise from multidisciplinary branches such as engineering, physics, chemistry, and biology, among others (**Figure** 1a). This field has different perspectives on dealing with medical, food, and environmental issues. One of the benefits of working with nanotechnology, especially nanomaterials, is to study and improve the interaction of biological systems at the nanometric scale for the convergence of intracellular processes like molecule transport and activation/deactivation of oncogenic pathways.[1,2] Materials can offer variable challenges and advantages depending on the application where they are employed. For instance, different materials are listed as suitable alternatives, such as CdSe, $TiSe_2$, CdTe, ZnSe, Cu_2S, AgBr, C, and Silicon (Si), which have been used as analysis tools in different biological science

A. Dutt, R. A. Salinas, C. D. Ramos, G. Santana
Instituto de Investigaciones en Materiales
UNAM
A.P. 70-360, Coyoacán, México City C.P. 04510, Mexico
E-mail: adutt@iim.unam.mx

S. E. Martínez-Tolibia
Departamento de Bioingeniería y Bioprocesos
Centro de Investigación en Biotecnología Aplicada del Instituto Politécnico Nacional (CIBA-IPN)
Tlaxcala 72197, Mexico

The ORCID identification number(s) for the author(s) of this article can be found under https://doi.org/10.1002/adpr.202300054.

J. R. Ramos-Serrano
Instituto de Física
Benemérita Universidad Autónoma de Puebla
14 sur y Av. San Claudio, Puebla C.P. 72570, Mexico

M. Jain, Y. Matsumoto
Departamento de Ingeniería Eléctrica
Centro de Investigación y de Estudios Avanzados del IPN
Av. IPN 2508, Col. San Pedro Zacatenco, México City C.P. 07360, Mexico

L. Hamui
Facultad de Ingeniería
Universidad Anáhuac México
Avenida Universidad Anáhuac 46, Col. Lomas Anáhuac, Huixquilucan, Estado de México 52786, Mexico

E. Mostafavi
Stanford Cardiovascular Institute
Stanford University School of Medicine
Stanford, CA 94305, USA
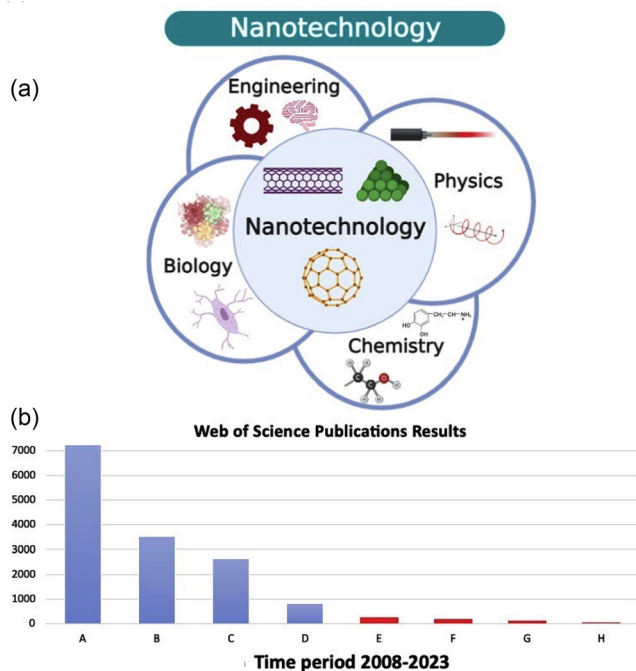
Figure 1. a) Schematic representation of nanotechnology and its relation with other research fields (*Created with Biorender.com*). b) The systematic search using the Web of Science platform; data are for the period from 2008 to 2023, the y-axis is the number of publications. A–H denote different search filters: A) Nanoparticles for Bioimaging, B) Quantum Dots for Bioimaging, C) Nanoparticles and Optical Diagnostics, D) Quantum Dots And Optical Diagnostics, E) Silicon Nanoparticles for Bioimaging, F) Silicon Quantum Dots for Bioimaging, G) Silicon Nanoparticles And Optical Diagnostics and H) Silicon Quantum Dots And Optical Diagnostics.

fields.[3–11] The perspective on semiconductors is comprehensive; however, the addition of nanoparticles (NPs) or nanocrystals (NCs) can potentiate their optical signal responses, offering enhanced performance in addition to the benefits mentioned earlier.

Especially talking about Si, it offers appropriate properties such as biocompatibility and biostability, providing lucrative opportunities to utilize them in biological systems. This

Y. Kumar Mishra
Mads Clausen Institute
NanoSYD
University of Southern Denmark
Alsion 2, 6400 Sønderborg, Denmark

V. K. Thakur
Biorefining and Advanced Materials Research Center
Scotland's Rural College (SRUC)
Kings Buildings, West Mains Road, Edinburgh EH9 3JG, UK

A. K. Kaushik
NanoBioTech Laboratory
Department of Environmental Engineering
Florida Polytechnic University
Lakeland, FL 33805, USA

manifests the significance of materials development that can potentiate, inhibit, detect, or provide a general overview of intracellular processes for monitoring the interaction between cells and nanostructures. A complete study and knowledge in this area could enable using Si-based nanomaterials in biomedical and biotechnological (i.e., imaging, bacterial detection, and inhibition) sectors. However, one of the main limitations of developing optical emitters, detectors, and imaging diagnostics devices based on Si technology (bulk form) is the indirect bandgap of this material.[12] This constraint makes Si a so-called "dark" material for luminescence applications because of its long radiative lifetimes and lower efficiency.[13,14] In general, the low photoluminescence (PL) efficiency of bulk c-Si in a near-infrared region is associated with its electronic band structure, generally represented by the dispersion relation, $E(\mathbf{k})$. This represents the electron (or hole) energy at the band edge, in terms of the crystal momentum or wave vector, $\mathbf{k}$, in the first Brillouin zone (BZ). The E versus $\mathbf{k}$ data calculated from empirical pseudopotential methods found that silicon structure is similar to a diamond lattice with an indirect-bandgap material.[15,16] The upper valence band (E_g) is centered at the BZ ($k = 0$), and each one of the equivalent minimal conduction band (E_c) is situated at $k = 0.86 \, \pi/a$, where a is the lattice constant of c-Si (5.4307).[17] On the other hand, below the effective mass approximation (EMA), electrons and holes can be considered freecharge carriers at the bottom of the conduction band and the top of the valence band, respectively, and the corresponding state densities are parabolic. One solution is to investigate and develop Si-based light-emitting sources (NPs and NCs) that could easily be integrated with the existing Si-based electronic circuit technology.[13]

After the first visible emission from pSi thin films, it was inferred that Si properties could be varied depending on the material dimensionality, discovering that the characteristics of its nanostructures could diverge hugely from their counterparts, that is, bulk structure.[18–20] This finding led to a worldwide investigation to explain and explore the optical responses from Si quantum dots (QDs), NPs, and NCs, among others.[21] It is imperative to mention that these different forms could be differentiated with the size distribution. For instance, for NPs, the size range is ≈0–100 nm; for semiconductor QDs (0–10 nm), and in the particular case of Si QDs, it is less than 5 nm to obtain confinement effects. Thus, depending on the size distribution and their applications, these different terminologies will be henceforward used in the present review. Likewise, when QDs and NPs are embedded in different surrounding matrices (oxides—SiO_x, nitrides—SiN_x, and carbides—SiC), one can control the size and density distribution and provide good passivation to the whole system (more details are provided in the subsequent section). Several investigations related to the structural, optical, and electrical analysis of Si-based nanomaterials have been explored and discussed in some of our recently published reports.[22–29] Now, keeping in mind the optical responses offered by Si-based compound nanomaterials (QDs, SiO_x, SiN_x, SiC) and the experience gained from our previous studies, we believe that the PL properties could be a linking point to the biological research. Moreover, in this review, the Web of Science database has been used to compile information about the number of literature reports in the area, in general, for bioimaging and optical

diagnostics. A particular search was realized for Si QDs and NPs for the afore-mentioned applications. To identify the relevant literature, multiple keywords, and term combinations were used, including "Nanoparticles for Bioimaging," "Quantum Dots for Bioimaging," "Nanoparticles And Optical Diagnostics," "Quantum Dots And Optical Diagnostics," "Silicon Nanoparticles for Bioimaging," "Silicon Quantum Dots for Bioimaging," "Silicon Nanoparticles And Optical Diagnostics," and "Silicon Quantum Dots And Optical Diagnostics," respectively (Figure 1b). It can be clearly seen that the tendency for the usage of Si-based compound nanomaterials is still limited in the area of bioimaging, and once we understand the optical properties of these complex compound nanomaterials, a new era of the research area could be explored for the early detection of diseases.

The present review highlights the properties of these multidimensional nanomaterials for attractive applications by understanding the complex topic of the PL mechanisms and also will present the state of art of Si-based compound nanostructures for bioimaging applications. Since materials type and their dimensions can modify the PL emission of Si nanomaterials, it is fundamental to evaluate their responses under different conditions to know how they could behave and adapt to diverse biological environments. In addition, some critical points, such as fabrication techniques and mass-scale production, are also briefly discussed, which will help researchers from different backgrounds to exploit Si QDs properties even more. At last, the role of Si in modern medical diagnostics, with an emphasis on lower-cost, prompt, and reliable response, early detection of diseases, and sophisticated therapy development (tissue), is presented.

2. Embedding QDs and NPs in Thin-Film Matrices and their Relative Properties

2.1. Why is the Need for Embedding Si Nanomaterials?

Over the last few years, various configurations and models have been used to grow Si-based compound thin films. As a result, different deposition and surface modification strategies are shown in **Figure 2** as a general overview of these nanomaterials and their applications. As shown, a classification is made based on relevant deposition techniques such as plasma-enhanced chemical vapor deposition (PECVD), low-pressure chemical vapor deposition (LPCVD), atomic layer deposition (ALD), as well as tailored surface modification methods (aqueous and vapor-phase), all of which have been applied for the development of microelectromechanical and nanophotonic devices, integrated circuitry (IC) and optical devices, chemically reactive electrodes, and biosensors.[30]

As mentioned, from p-Si, it was inferred that Si properties could be varied depending on the material dimensionality, discovering important characteristics of these nanostructures. However, some investigators found that p-Si had some limitations, such as instability and fragile nature, because of its high surface area, broad particle size distribution, and poor photochemical stability.[31–33] Therefore, the need to embed Si NPs in the host matrices was first evidenced in 1994.[31] Then, the search for new production techniques to control the morphological characteristics, such as particle size, and to attain the stability of embedded NPs, was investigated.

A chemical synthesis that produces a colloidal dispersion with reasonable size control is one of the most widely used techniques
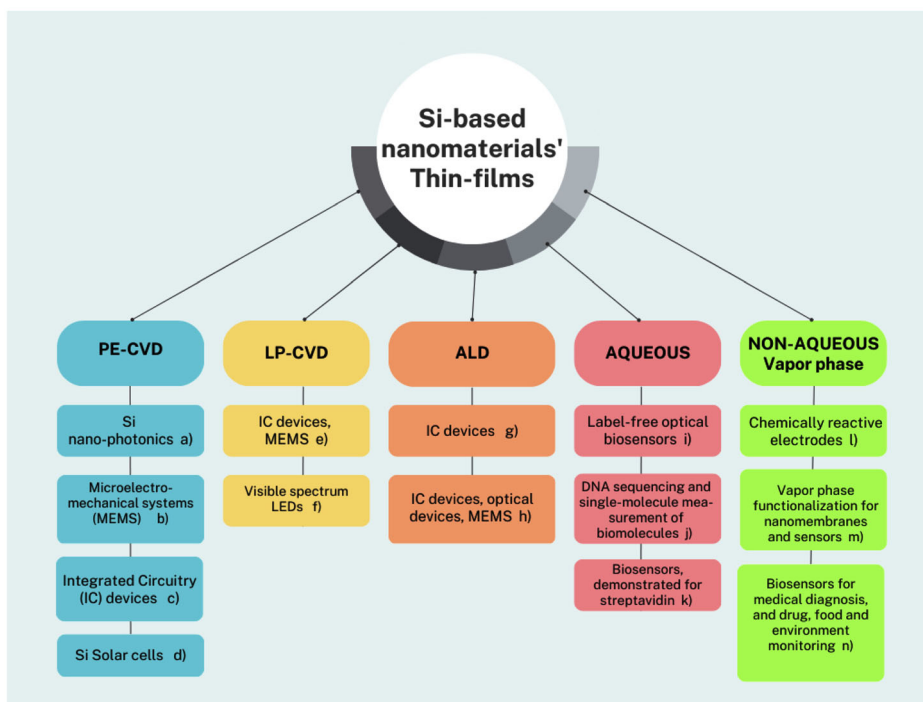
Figure 2. Schematic summary of the main configurations of Si-based nanomaterials based on deposition techniques and their applications. References are numbered as indicated: a)[100,218,219], b)[220–222], c)[222–224], d)[225,226], e)[227], f)[228], g)[229], h)[230], i)[231], j)[232], k)[233], l)[234], m)[235], n)[236].

for obtaining Si-based compound nanomaterials. This technique is ideal when the fabrication of QDs and NPs at low temperatures is required.[11] Afterward, the growth of nanostructures embedded in these matrices was developed using ion implantations followed by postdeposition heat treatment methods, reporting a successful PL emission.[34–36] In this method, excess Si was precipitated as NPs (or QDs when they were smaller). In comparison, Si ultrathin films immersed in different dielectric matrices (SiO_x, SiN_x, and SiC) and their oxide forms (SRO silicon-rich oxide, SRSO silicon-rich silicon oxide, SiO_xN_y, SiO_xC_y) have proven to be the best options to obtain Si-based compound nanomaterials by depositing nonstoichiometric films.[36–44] It is well known that embedding NPs and QDs in these matrices could substantially change the structure's optical and electrical properties.[45]

Regarding the characteristic features of each dielectric matrix and their applications, previous eports describe the increase in the refractive index (RI) by increasing the Si amount in these Si-rich dielectric matrices.[37–41] Some investigators used this property for designing planar waveguides, allowing the development of on-chip photonic devices.[46] In addition, when dielectric matrices (with a wide bandgap) surround Si NPs, this enables the electron–hole pair confinement in the NPs, QDs, and the overall system could display the quantum confinement effect (QCE). The luminescence related to QCE in these materials has attracted attention due to the intense PL in a vast spectrum region from infrared (IR) to ultraviolet (UV).[28,47,48]

QDs with a diameter lower than the Bohr radius and narrow size distribution exhibit higher PL intensity due to a more significant localization of electrons and holes in a confined area, thus, increasing the probability of radiative recombination. In the case of PL properties, it has been shown that QDs embedded in an oxide matrix have PL energy less than 2 eV; on the other hand, for nitride matrix, they have PL energies between 1.5 and 2 eV **(Figure 3**a), and near 3 eV, as shown later in Table 2. SiO_x matrix shows a reduction in PL owing to the structure distortion caused by a double oxygen bond. Hence, the SiN_x matrix is considered more stable due to the better passivation by nitrogen atoms. Discussion about complex luminescence mechanisms is the key delivery point of this review, and detailed discussions can be found in the succeeding sections. As mentioned earlier, it is well known that the overall optoelectronic properties of Si QDs and NPs could also vary extensively depending on factors such as their size distribution, spacing between them, and the embedding matrix.[49] The barrier height is also one of the decisive factors for optoelectronic properties such as conductance.[50] The lower barrier height in SiN_x and SiC matrices makes them more conductive than SiO_x (Figure 3b).[51] Figure 3c–e shows the PL emission of Si QDs embedded in SiO_x, SiN_x, and SiO_xC_y matrices.[22,27,52] Figure 3c shows the effect of annealing treatments on the QDs size distribution and hence, the control over different emissions at the visible region. It can be seen that different heat treatments induced a size change that further invoked the confinement effect, and overall an indirect-bandgap material was able to emit in different regions. Then, Figure 3d represents a solid visible emission from Si QDs embedded in the SiN_x matrix, observed after irradiation with a 325 nm source. Lastly, Figure 3e shows a white emission from Si QDs in SiC deposited by organic catalytic chemical vapor deposition (O-Cat CVD).

Conceivably, PL property motivated the development of electroluminescent devices (ELDs) based on Si-rich dielectrics; the first attempts were made on SRO thin films.[53] For designing modern optoelectronic applications, it must be kept in mind that injecting charge carriers into SRO and other oxygen-rich matrices is difficult due to their wide bandgap and low mobility. In that case, nitride and carbide are proposed as alternatives due to their lower barrier height and higher mobility.[25,49] Another prospect for these Si-compound thin films is their application to improve solar cell efficiency as antireflective or downshifting layers, which absorb UV radiation and re-emit it in the visible region.[54] Recently, Si NPs have been tested in different structures to develop photovoltaic devices, such as n-type Si QDs/p-type c-Si heterojunction, p-type Si QDs/n-type c-Si heterojunction, and p–i–n diodes.[55,56] Efficiencies below 15% have been reported in structures of these types; however, the main limitation is still the difficulty of transferring the electric charge due to dielectric matrices.[57] A brief comparison of the properties reported for Si-related matrices is summarized in **Table 1**.

The following sections thoroughly discuss the PL properties of Si NPs and QDs in three matrices. As seen in the discussion before, the dimensionality of these matrices provokes some critical changes in QD confinement. In summary, this review collates the PL mechanisms of Si NPs embedded in the different matrices and their respective properties, highlighting their usage for remarkable upcoming applications. Moreover, the potential of Si-based compound thin films is presented for ultrasensitive biomolecular detection and dynamic imaging analysis, with motivation on real-time detection.

3. Emission Mechanisms of Si Nanostructures in the Oxide-Related Matrix

As mentioned earlier, in 1990, foremost, intense visible emission from green to red color was observed from porous Si nanostructures (SiO_2) when excited with a UV laser (3.1 eV),[20] observed later by Chiodini et al. (3.7 eV).[58] Afterward, other researchers observed the relation between the optical absorption of 2D nanostructures and NPs size, finding that the smaller particles tended to emit light at higher-energy values (shorter wavelength).[59] Though many reports have described the visible emission of Si NPs, and QDs in oxide matrix, the emission mechanisms are still under debate between surface defect states and the QCE.[60,61] More details regarding these two mechanisms have been provided in the following sections.

3.1. Quantum Confinement Effect (QCE)

The QCE in semiconductor materials, especially those with an indirect bandgap, has got much interest as it significantly modifies their electronic band structure. In the case of Si, this principle was first explained by Canham, which states that when the size of Si NPs is sufficiently small (i.e., <5 nm order of Coulombic exciton radius), the photogenerated electron–hole pairs can get trapped inside the resultant quantum well and could emit in the visible instead of the infrared region (bulk c-Si).[19] In that case, energy levels for the trapped exciton pairs are inversely proportional to the quantum width well, depending
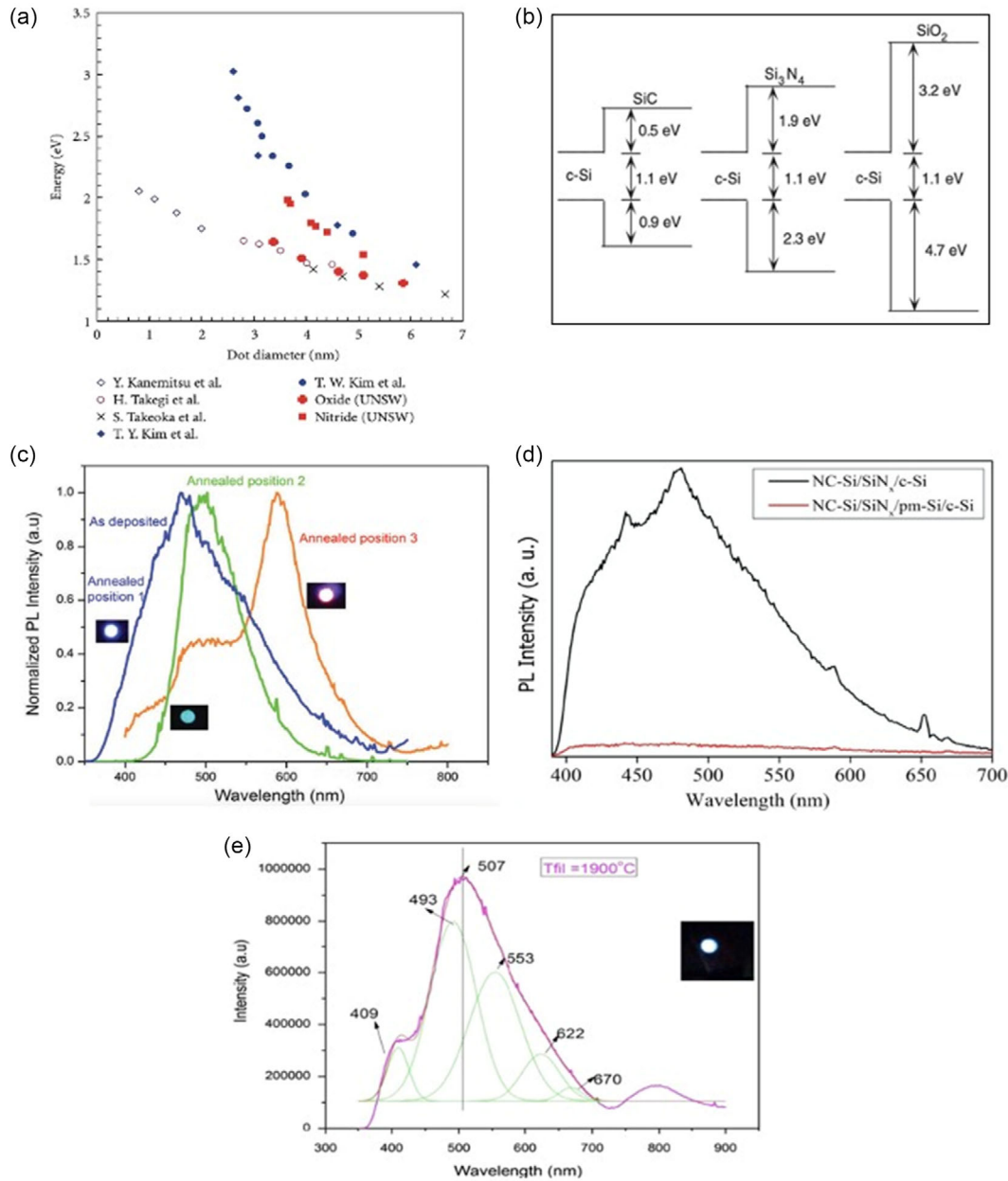
Figure 3. a) Energy gaps of 3D-confined Si NCs in SiO$_2$ and SiN$_x$ matrices. Reproduced with permission.[237] Copyright 2007, Hindawi. b) Bandgap of oxide, nitride, and carbide matrix alignments. Reproduced with permission.[51] Copyright 2006, Elsevier. c–e) PL emission of Si QDs in different matrices. Reproduced with permission.[22,27,52] (c) SiO$_x$, Copyright 2017, RSC; (d) SiN$_x$, Copyright 2017, Elsevier; (e) SiO$_x$C$_y$, Copyright 2015, Elsevier, respectively.

on the Si NPs size. After discovering QCE in NCs, other configurations such as porous, free-standing NPs, Si NPs, QDs embedded in SiO$_2$, and Si/SiO$_2$ superlattices have also been studied for a range of applications.[62] To explain this effect, we can substitute the term exciton pairs with wave functions related to these species, confined in a potential well of defined thickness. In brief, it could be stated that, with the decrease in Si NPs size (decreasing the size of the potential well), the ground-state energies are henceforth increased, also resulting in an increment of the bandgap, which is further correlated with the formation of discrete energy levels (**Figure 4**).

From Heisenberg's uncertainty principle, direct transitions caused by the spreading of the wave function in momentum space could be explained, and also, the increase in the gap energy in that particular case is clear from the following relation

$$\Delta E_{\mathrm{g}} = \frac{\hbar^2 p^2}{2MR^2} \tag{1}$$

where R is the Si NP size, M is the effective exciton mass, p is momentum, and $\hbar$ is a constant. Thus, a shift in the higher energies (shorter wavelength) of emission spectra is direct evidence

Table 1. Summary of optical and electrical properties commonly reported for si matrices.

Matrix Type	Refractive index n at 632.8 nm	Maximum of PL emission [eV]	Mobility [cm² V⁻¹ s⁻¹] (2 nm crystal size and inter-dot distance)
Silicon carbide (SiC)	2.7–3.0[240]	2.2–2.7[241]	10^2[49]
Silicon oxide (SiOₓ)	1.4–2.7[242]	1.9–2.8[243]	10^{-2}[49]
Silicon nitride (SiNₓ)	1.9–2.2[70]	2.0–2.6[24]	1[49]
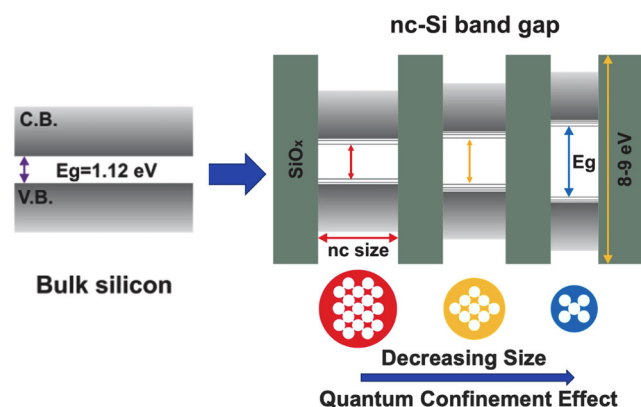
Figure 4. An illustratory diagram of the difference in the bulk and Si QDs bandgap, highlighting the QCE concept.

of QCE.[63] However, calculating the gap energy for Si-based compound thin films is a complex process. Several approaches and models, like EMA, empirical pseudopotential approach (EPA), and tight-binding scheme, are considered. EMA is one of the most used models, which explains the concept straightforwardly. There are numerous studies regarding the dependence of Si QDs size and PL peak energy; however, an association between the peak photon energy (in eV) and QDs diameter (in nm) is under the following equation[64]

$$E = 0.925 + \frac{3.73}{d^{1.39}} + \frac{0.881}{d} \tag{2}$$

Later, Delerue et al. proposed another relation for this association, $E_{pl} = E_g + (3.73/d^{1.39})$, where E_g is the bandgap of Si bulk, and d is the average diameter of NC.[65]

In summary, the significant repercussions of QCE on nanostructures are 1) broadening of wave factors, making the structure similar to a direct bandgap, that is, no need of phonon for inter-transitions; and 2) It also results in a bandgap widening. This similarly causes an increase in the emission intensities due to the small size of NPs with well-defined energy levels.

3.2. Surface and Interface States

Koch et al. explained that besides QCE, other complex situations could occur inside the NPs and QDs.[66] Still, photon absorption happens inside, but exciton pairs' recombination could occur in different localized states. In the first case, transitions and recombinations can occur as usual, resulting in band-to-band radiative recombinations (QCE). In the second case, it could also occur in the form of a band-to-surface state (defect state), and in the third case, it could show a surface-to-surface recombination process (electrons and holes are confined in distinct surface states). This model states that PL intensity dramatically depends on the NPs and QDs size (experiments performed under fixed PL peak position at 1.7 eV).[62] In 1993, another theoretical model was deduced to explain the emission at 1.7 eV, establishing that energy absorption still occurs inside the Si core. Once more, the exciton pairs move out to the interface between the Si NPs and host matrix layer (SiO₂) to recombine radiatively. In this case, a quantum well is formed due to the bandgap mismatch between the Si and oxide layers, but the quantum well width is independent of NP size.[67] Other authors also present similar structure types, as shown in **Figure 5**. The authors suggested the band alignment of Si NPs embedded in the SiO₂ matrix (Figure 5a). After calculations, they found a value close to 1.7 eV reflecting the role of the confinement region and surface states.[68] Figure 5b shows the proposed PL mechanisms for the green emission from the SiOₓ matrix. As shown, different
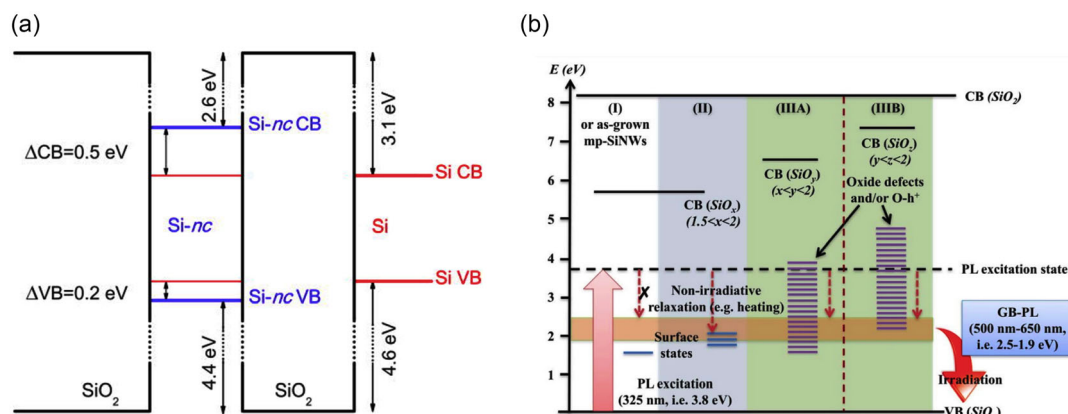


Figure 5. a) Band diagram of Si NPs (mean diameter of 2.6 nm) embedded in SiO₂ matrix. Reproduced with permission.[68] Copyright 2011, AIP. b) Representation of the different interface states and transition levels between the valence and conduction bands, giving rise to distinct color emissions. Reproduced with permission.[69] Copyright 2014, Springer Nature.

**ADVANCED
SCIENCE NEWS**

www.advancedsciencenews.com

**ADVANCED
PHOTONICS
RESEARCH**
Open Access

www.adpr-journal.com

regions have been marked (I), (II), and (III), showing the importance of varying interface states for the visible emission from the oxide matrix. Relative energy levels are crucial and influence the complex structure's emission properties.[69]

Other experiments were performed, finding that even after carrying out various annealing or oxidation conditions, PL was always observed close to 1.7 eV. At last, it was confirmed that this peak at 1.7 eV was independent of Si NPs size, and defect states such as P_b ($Si_3 \equiv Si \cdot$ defects) were causative of this emission.[59,60,70] One possibility to distinguish defect sites is using electron spin resonance (ESR) technology. The crucial observation from these experiments is that PL emission is not size dependent on Si QDs (≤ 3 nm) embedded in the SiO_2 matrix.

Under this regime, an exciton recombination could occur from the interface states formed inside the bandgap of QDs. Additionally, when Si QDs are embedded in an oxide matrix (SiO_x), distinct centers such as Si–H (hydrides) bonding states, oxygen-deficient centers (Si–Si), nonbridging oxygen centers (SiO), surface-trapped excitons, and/or dangling bonds can also provoke emission from thin films.[24,27,29] Moreover, passivation types (saturation of terminal bonds with hydrogen and oxygen species) are also critical for emission mechanisms as well. Therefore, the passivation of Si QDs is an essential parameter for the final PL properties, as shown in **Figure 6**.

Figure 6a shows the PL spectra of Si QDs when excited with a source (4.4 eV) under different oxidation levels and
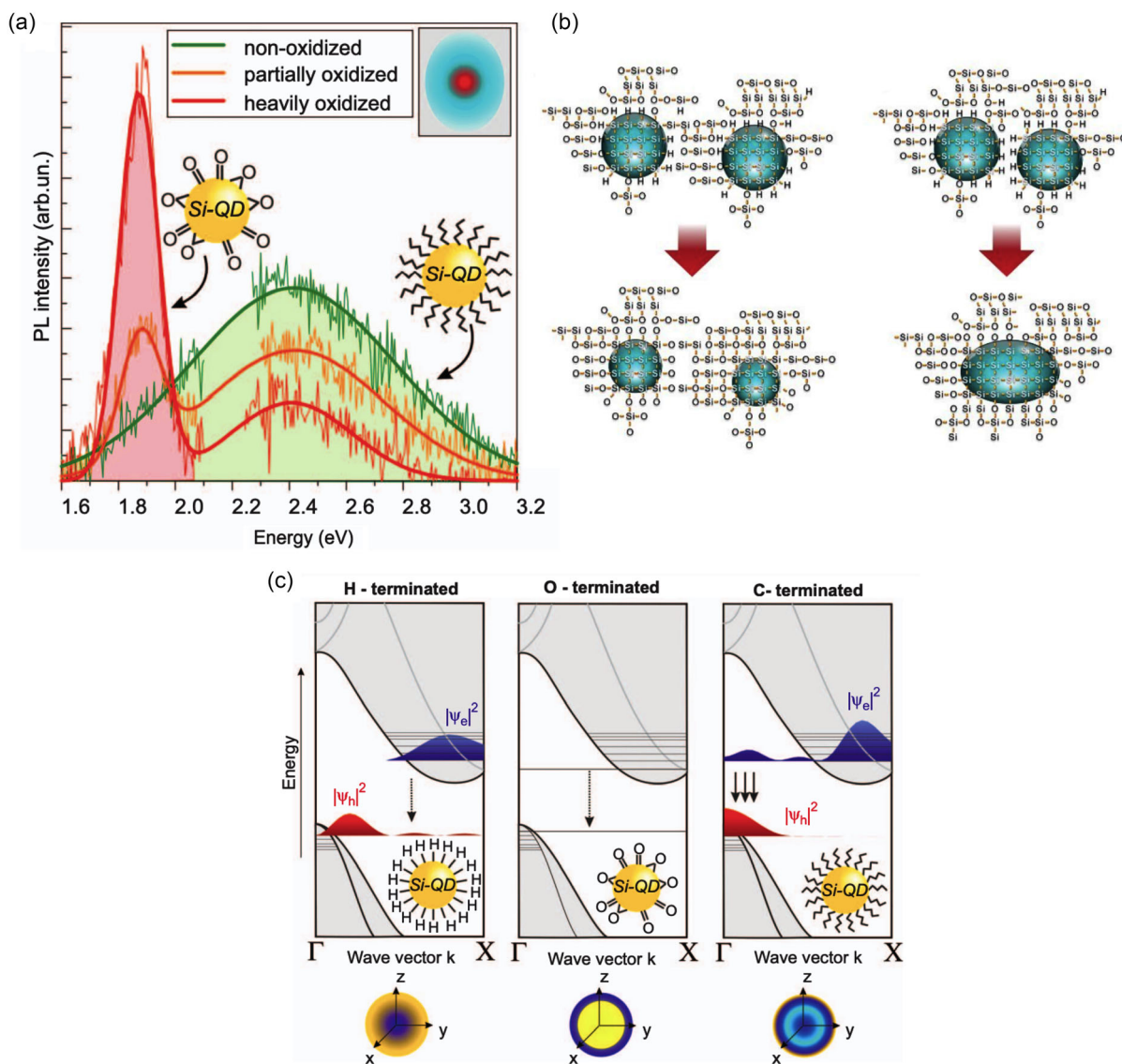
Figure 6. Effect of different passivation environments on Si QDs. a) Role of oxidation on the PL intensity. Two main contributions around 1.8 and 2.4 eV can be seen from oxidized samples. PL spectra of C-terminated (green), partially oxidized (orange), and heavily oxidized (red) Si QDs. The inset illustrates the illuminated spot (blue) and the photooxidized area (red). Reproduced with permission.[71] Copyright 2013, Springer Nature. b) Passivation of Si QDs under different conditions resulting in overall changes in the size of QDs. Reproduced with permission.[27] Copyright 2017, RSC. c) Illustration of the radiative channels in H–, O–, and C– passivated Si QDs. Reproduced with permission.[71] Copyright 2013, Springer Nature.

C termination by oxygen.[71] As observed, oxidation provokes significant changes in the PL intensity and position. This could also be a surplus when different color emissions for respective QDs applications are desired. Figure 6b presents a suitable model where QDs are passivated under different circumstances, such as partial O and partial H. It was also observed that QDs size is either incremented or decreased depending on the condition.[27] and consequently, changes can be measured in the final bandgap of the material. Figure 6c shows the radiative rates of excitonic recombination in QDs, in terms of the electron and hole densities distribution in the real and k-space. It was observed that H– and O– terminated QDs show slow radiative PL. In comparison, regarding C- terminated QDs, the rate is increased due to less participation of phonons in the process. The aforementioned discussion illustrates that not only the size but the surrounding environment is also very influential on the optoelectronic properties of QDs.[71]

3.3. Other Mechanisms

As mentioned above, other mechanisms can cause emission in Si-based thin films, such as oxygen deficiency center (ODC), which causes the particular emission at 2.7 eV.[72] **Figure 7**a Nonbridging oxygen hole center (NBOHC) with a specific emission at 1.85 eV.[73–76] and particularities such as full width half maximum (FWHM) of 0.17 eV and decay constant of 20 μs is observed in Figure 7b.[60] The existence of self-trapped exciton (STE) results in characteristic emissions in the range of 2–3 eV (Figure 7c). E' center could present different emission bands between 2.7 and 3.7 eV (460–335 nm) (Figure 7d). Finally, hydrogen-related surface species could exhibit specific emissions in the visible region (2.3 eV) related to siloxene and SiH_2 bondings.[77,78]

3.4. Complexity among Different PL Mechanisms

Looking over all the possible emission mechanisms related to Si NPs and QDs embedded in an oxide matrix, it is understandable that recombination and radiation are very complex procedures. One cannot expect a single process, for example, QCE depending on the particle sizes because there are many dichotomies between the diverse mechanisms. All these surface states, like
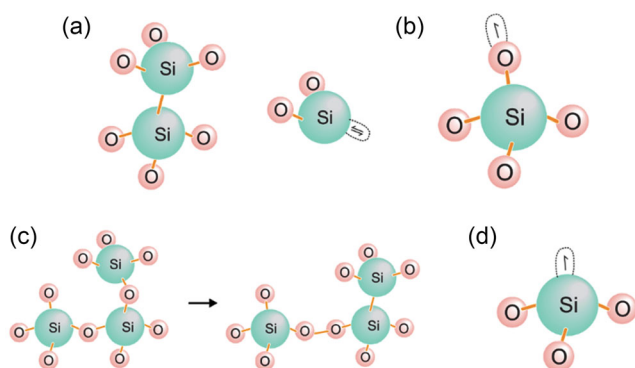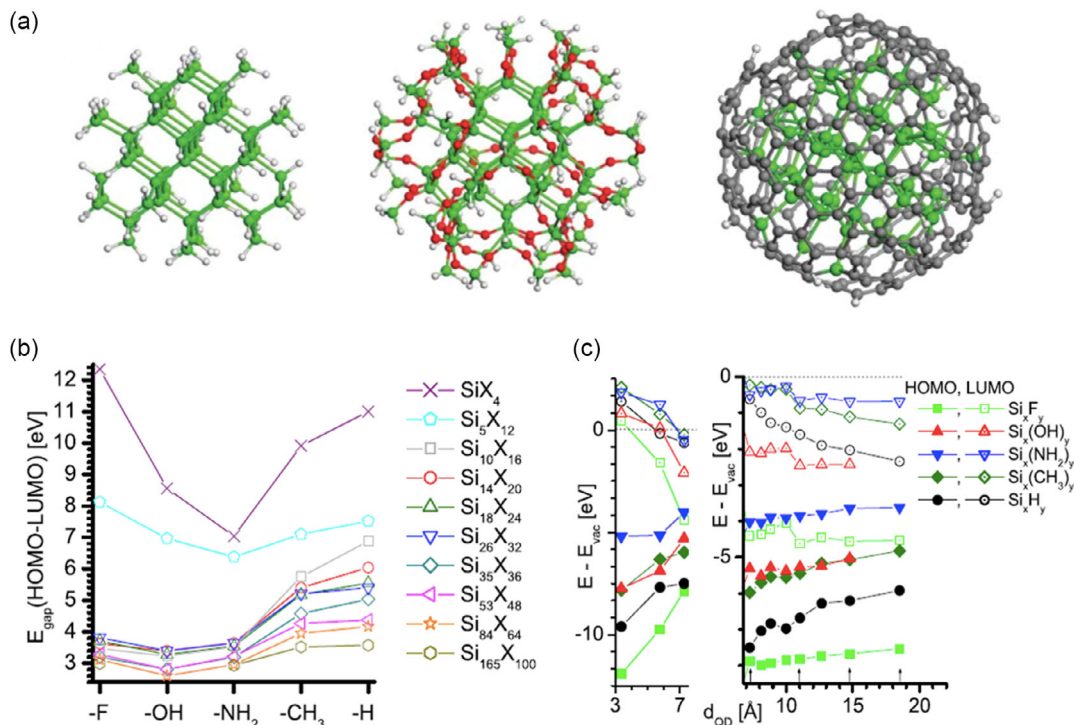
NBOHC, STE, ODC, and hydrogen-related defect sites, participate parallely with the QCE model. Even as presented in a previous report, disagreement was found in the PL peak energy in correlation with the NPs size, which provided evidence regarding the complexity of this phenomenon.[79] As the size of NPs decreases, it helps to extend the bandgap. Thus, it causes the generation of many interface states between the valence and conduction bands. It is evident that the emission from Si NPs and QDs embedded in an oxide matrix is multifaceted. There is always a chance of hopping exciton pairs between various energy levels related to the particle sizes or at different surface/defect states (Figure 5b). In contrast, these energy levels could also be correlated with diverse defect states, as discussed earlier. Advanced optical characterizations, such as time-resolved PL (TRPL), could always help to interpret the precise mechanisms behind the emission of Si-based compound thin films.[29]

4. Hydrogen Passivation Effect on PL Emission

Despite different approaches and materials widely used for Si-based light source fabrication, their emission efficiency is limited by general physical properties, such as defects in the host matrix.[80] Nevertheless, when considering the presence of hydrogen in Si electronic devices, several investigations have shown its ability to passivate the dangling bonds present in the matrix, directly impacting the device's stability, optoelectronic properties, and electrical output, among others. It is well known that hydrogen passivation allows the adjustment of Si NPs and QDs optical properties, modifying the chemistry of the surface and revealing an efficient emission.[81–85] Wilkinson et al. observed that good passivation of Si NPs enhances their luminescence efficiency.[83,86,87] However, dangling bond defects could reduce the overall luminescence due to its nonradiative behavior.[65,88–93] Thus, hydrogen passivation is crucial for increasing nanocrystal luminescence; additionally, understanding the passivation process allows maximum luminescence efficiency. On the other hand, hydrogen-passivated Si NPs have shown dispersibility, and oxidation resistance is enhanced in these cases.[94] The model of hydrogen-passivated Si NPs ($Si_{71}H_{84}$) embedded in SiO_2 is shown in **Figure 8**a.[84] Moreover, surface hydrogenation is also crucial due to the absence of oxygen atoms bonded to the NPs affecting the luminescence mechanisms.[80,95,96] The effect of hydrogen passivation with respect to other elements and the impact of the NPs symmetry on E_{gap} highest occupied molecular-orbital-lowest unoccupied molecular-orbital (HOMO-LUMO) can be observed in Figure 8b,c.[83]

Different hydrogen passivation techniques can be employed, such as ion implantation of hydrogen or deuterium, laser ablation, post-thermal treatment, and postmetallization annealing process with Al (known as alneal) and Cr, but the most used is thermal annealing in forming gas. This can improve the passivation of interfaces compared to the other techniques due to the formation of a large amount of atomic hydrogen. The annealing treatment parameters, like temperature, environment, and duration, affect the radiative recombination of NPs and QDs.[97,98] Thus, the thermal H_2 passivation can be modeled by essential chemical reactions as follows

Figure 7. Schematic models for different defect states. a) ODC(I) and ODC(II), b) NBOHC, c) STE, and d) E' center.

Figure 8. a) Model results for passivated Si NPs, with H, SiO$_2$, and C, of 1.4 nm diameter. Reproduced with permission.[84] Copyright 2012, RSC Publishing. b) HOMO–LUMO gaps of SiX$_x$. Reproduced with permission.[83] Copyright 2008, APS. c) QD diameter is dependent on HOMO and LUMO energies. Reproduced with permission.[83] Copyright 2008, APS.

$$P_b + H_2 \xrightarrow{k_f} P_bH + H \tag{3}$$

$$P_bH \xrightarrow{k_d} P_b + H \tag{4}$$

where

$$k_f = k_{f0} e^{\frac{-E_f}{KT}} \tag{5}$$

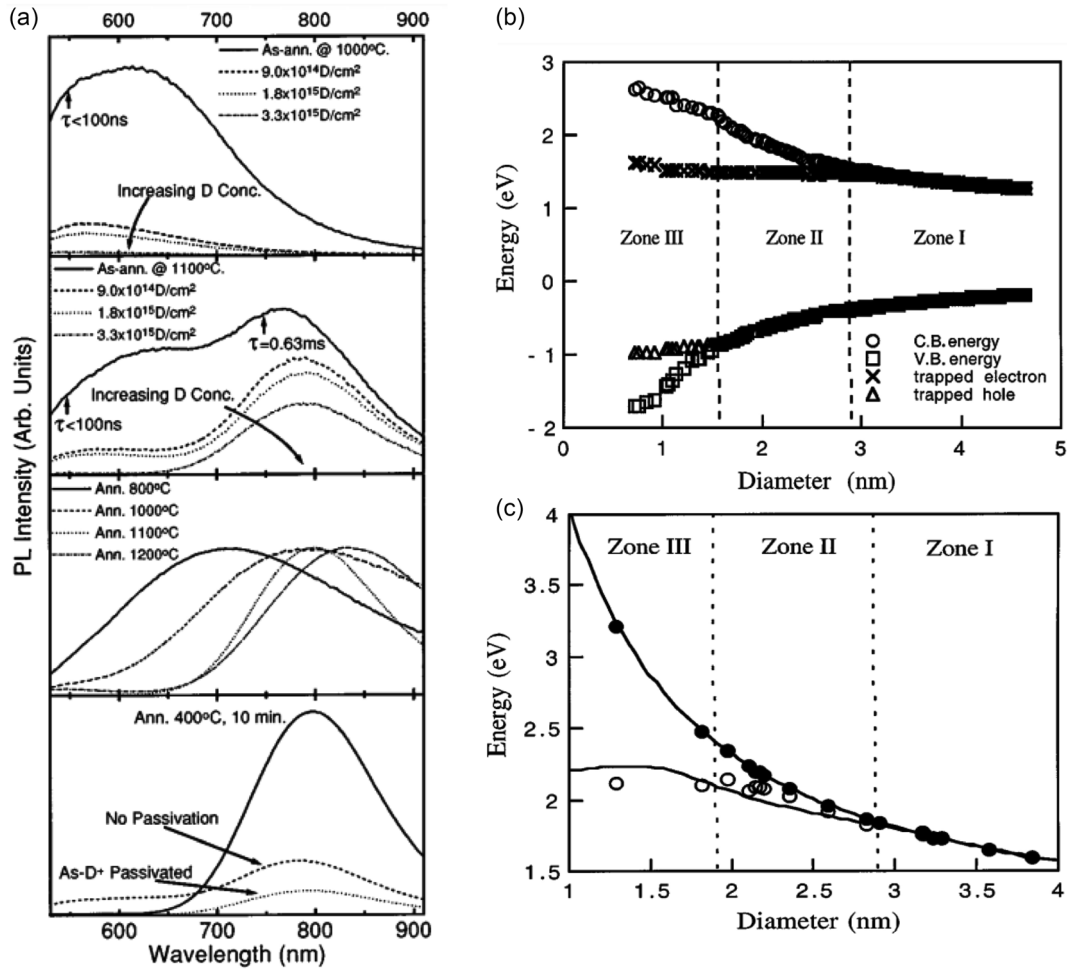$$k_d = k_{d0} e^{\frac{-E_d}{KT}} \tag{6}$$

Other passivation techniques have shown different behaviors. For instance, the PL spectra from NPs (implantation of 50 keV Si ions on SiO$_2$ matrix and post-annealed) after deuterium implantation have been demonstrated to reduce the defect band (**Figure 9**a). Moreover, the increase in deuterium concentration presents a decrease in the NPs PL intensity. Further, thermal annealing induces deuterium diffusion, which augments the PL intensity, passivating the NPs. Even though for temperatures higher than 500 °C, the passivation effect is reduced due to the out-diffusion of deuterium.[99] As discussed earlier, PL spectra in Si NPs embedded in matrix materials are mainly composed of QCE and other mechanisms based on models that consider the interface between NPs and the matrix or surface states perturbed by passivated hydrogen bonds.[83,100,101] The emission mechanisms for Si NPs embedded in different matrices are quite complicated, considering that they own a highly reactive surface.

Several models have explained the absorption and luminescence of these materials because hydrogen-terminated surfaces are susceptible to oxidation. However, the emission is influenced by localized defect states' interface and excitons' quantum confinement.[83,102,103] The photogenerated carriers diffuse through a thermally activated mechanism to the surface of NPs, where confined excitons produce the PL radiation by one of these models. On the surface state model, absorption occurs in the NPs, and recombination occurs at the passivated surface via localized defects states.[87,101] Based on these models, Wolkin et al. calculated the NP size and surface passivation-dependent energy band structure. In contrast, the NP size becomes smaller, and the surface states could play a prominent role (Figure 9b). Also, in Figure 9c, it is observed that in the presence of oxide bonds, a blueshift is perceived for hydrogen-passivated NPs.[79] In summary, hydrogen passivation, surface hydrogenation, defect sites, and size dependency could induce changes in PL emission in nanostructures, which could be advantageously adapted to biological environments to detect PL emission change responses under different conditions.

5. Emission Mechanisms of Si Nanostructures in the Nitride-Related Matrix

The first works that reported the QCE of a particle in a box were based on the development of a simple model, which allows obtaining an analytical expression that correlates the NPs size L and confinement type (1D, 2D, 3D) with the bandgap energy values and/or PL peaks position.[104–106] The expressions to

**ADVANCED
SCIENCE NEWS**

www.advancedsciencenews.com

**ADVANCED
PHOTONICS
RESEARCH**
Open Access

www.adpr-journal.com

Figure 9. a) Room-temperature visible PL spectra of implanted SiO_2 films with D passivation postannealing. Reproduced with permission.[238] Copyright 1996, AIP Publishing. b) NPs' size and surface passivation are dependent on electronic states. Reproduced with permission.[79] Copyright 1999, APS. c) NPs size-dependent energy bands and the PL energy position. Reproduced with permission.[79] Copyright 1999, APS.

obtain the energy shift ΔE and the confined gap (E_{qcg}) and/or PL energy (E_{PL}) of a confined semiconductor NP with infinite potential barriers, considering the simple effective mass approximation with electrons and holes with effective mass m_e^* and m_h^*, are shown under the following equations.

$$\Delta E = \frac{\pi^2 \hbar^2}{2m^* L^2} \qquad (7)$$

$$E_{PL} = E_g + \frac{\pi^2 \hbar^2}{2L^2}\left[\frac{1}{m_e^*} + \frac{1}{m_h^*}\right] \qquad (8)$$

where the confinement constant C is given by

$$C = \frac{\pi^2 \hbar^2}{2}\left[\frac{1}{m_e^*} + \frac{1}{m_h^*}\right] \qquad (9)$$

Owing to their simplicity of fabrication and the advantage that QCE is three times higher in the 3D than in the unidimensional case (quantum wells), Si NPs embedded in a dielectric matrix have attracted higher interest than other superlattice systems.

Previously, it was described that optimizing the photoluminescent properties in SiO_x has significantly advanced. However, developing efficient optoelectronic devices is still a constant technological challenge. This derives from the difficulty of injecting charge carriers related to their high potential barrier. On the other hand, highly applied electric fields are close to the dielectric soft-breakdown region, significantly shortening the life of the device.

Si NPs and QDs embedded in a silicon nitride matrix (SiN_x) are another interesting Si-based material that displays intense PL. Besides showing a better capability for tuning the PL of embedded Si NPs and QDs, the SiN_x matrix is an alternative to SiO_x for the fabrication of ELDs because it presents a lower barrier for carrier injection (electrons and holes) during the operation of these ELDs compared to SiO_x.[107–109] SiN_x thin films can be prepared by diverse techniques. However, the selection of any deposition technique is determined by various factors such as cost, control of deposition parameters, film quality, and in this case, scalability to the existent CMOS infrastructure. **Table 2** summarizes the different methods for obtaining Si QDs embedded in the SiN_x matrix and some of their related properties.

Table 2. A summary of preparation methods, PL emission band, and related emission mechanisms of si QDs in SiN$_x$ matrix.
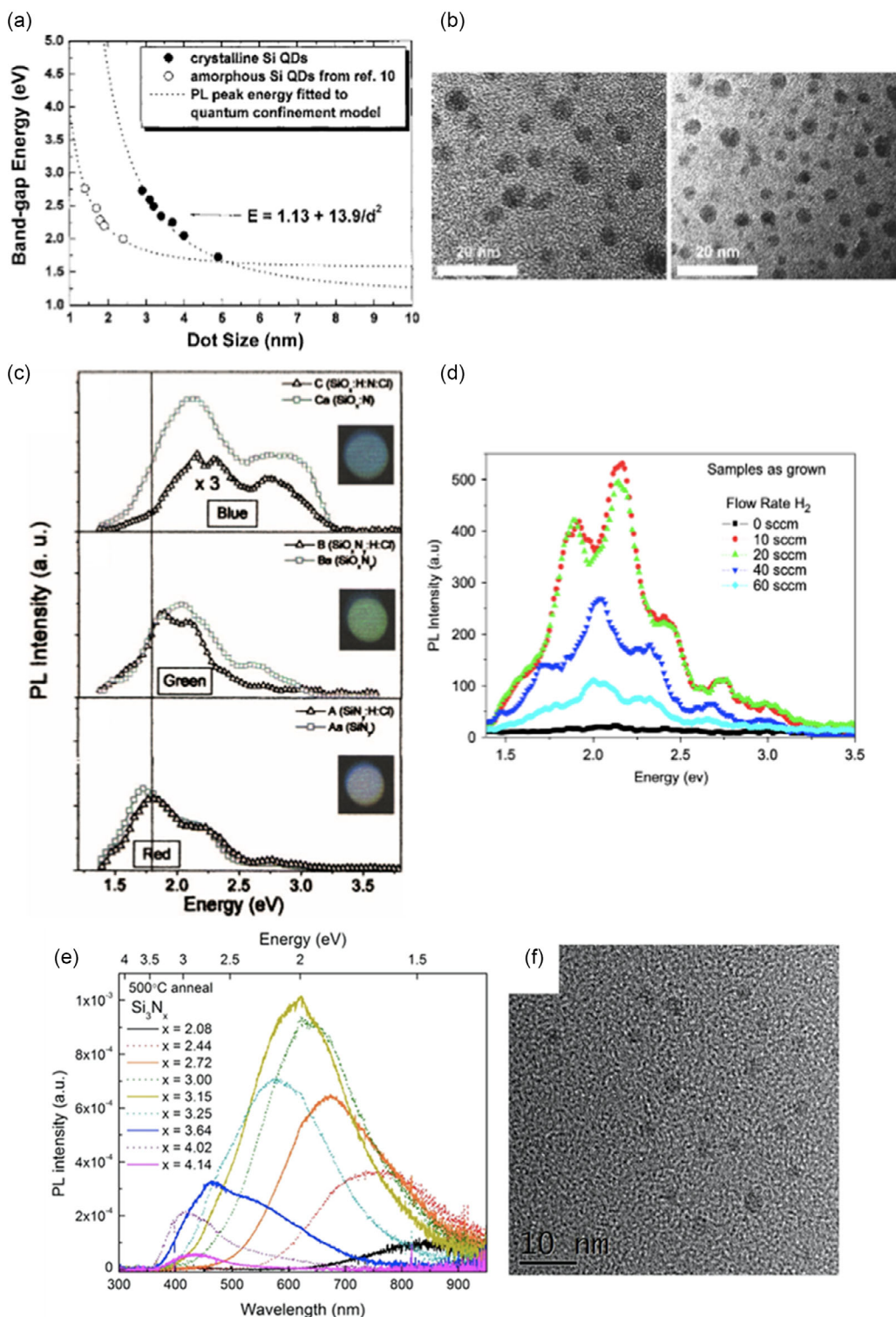
Synthesis method	Precursors	PL [eV]	Properties	References
PECVD[a]	Silane (SiH$_4$) + Ammonia (NH$_3$)	1.5–2.0	Si-rich cluster surrounded by N—H and Si—H bondings	[244]
LICVD[b]	SiH$_4$ + NH$_3$	3.2, 3, 2.8, 2.7, 2.4, 2.3, and 2.0	$\equiv$Si^0 → E_v (3.2), N–Si–O defects (3), Oxide defects (2.8), $\equiv$Si$^-$ → $=$N$^-$ (2.7), E_C → $\equiv$Si^0 (2.4), $\equiv$Si^0 → $=$N$^-$ (2.3) and E_C → $\equiv$Si$^-$ (2)	[245]
HFCVD[c]	Disilane (Si$_2$H$_6$) + NH$_3$	2.5 ± 0.1 and 3 ± 0.1	Silicon (2.5 ± 0.1) and nitrogen (3 ± 0.1) dangling bond defect	[246]
LPCVD[d] implanted with nitrogen ions	SiH$_4$ + NH$_3$	1.7–2.9	Amorphous silicon nitride intrinsic defects (N-centers)	[228]
VHF-PECVD[e]	SiH$_4$ + NH$_3$	2.17	Radiative centers related to the Si dangling bonds (K0) and N$_4^+$ or N$_2^0$.	[247]
PECVD[a]	SiH$_4$ + Nitrogen (N$_2$)	3.15–3.95 (Excitation range 3.35–5.16 eV)	STEs and energy transfer to donor-acceptor pairs.	[248]
PECVD[a]	SiH$_4$ + N$_2$	1.25 – 1.45	Amorphous and crystalline silicon nanoclusters	[249]
Heavy-Ion-Irradiated PECVD[a]	SiH$_4$ + N$_2$	1.82, 2.04 and 2.25	QCE (1.82), K-centers (2.04) and N-centers (2.25)	[250]
PECVD[a]	SiH$_4$ + N$_2$	1.9–2.9	Band tail states and K- and N-center	[219]
APCVD[f]	SiH$_2$Cl$_2$ + NH$_3$	2.53 and 3.29	QCE (2.53) and surface states around Si QDs (3.29)	[251]
PECVD[a]	SiH$_4$ + NH$_3$	1.6–2.73	Band tail states	[252]
PECVD[a]	SiH$_4$ + N$_2$	1.7 and 2.3	Tail-to-tail recombination (1.7) and direct band-to-band recombination (2.3)	[253]
PECVD[a]	SiH$_4$ + NH$_3$	2.45–3.1	QCE (QCE) and radiative defects	[254]
LPCVD[d]	Si$_2$H$_6$ + NH$_3$	1.84, 2.01, 2.10, 2.22, and 2.42	Amorphous silicon nanodots (1.84), Si-NPs (2.01), silicon (2.10) and nitrogen (2.22) defects and the amorphous matrix (2.42)	[255]
RPECVD[g]	SiH$_2$Cl$_2$ + H$_2$ + Argon (Ar) + NH$_3$	2.37 and 2.7	Interference effects (2.37) and Si QDs (2.7)	[256]
PECVD[a]	SiH$_2$Cl$_2$ + NH$_3$ + Ar	2.58	QCE	[257]
LPCVD[d]	SiH$_4$ + NH$_3$	2.0	Intrinsic defects (N centers)	[228]
PECVD[a]	SiH$_4$ + NH$_3$	1.9, 2.4 and 3	QCE (1.9), Si dangling bonds (2.4) and Nitrogen defects (3)	[258]
PECVD[a]	SiH$_4$ + NH$_3$ + N$_2$	2.15	Interference effect	[259]

[a]PECVD; [b]Laser-induced chemical-vapor-deposition technique; [c]Hot filament chemical vapor deposition technique; [d]LPCVD; [e]Very-high-frequency PECVD; [f]Atmospheric pressure chemical vapor deposition; [g]Remote PECVD.

The PECVD techniques for these thin-film preparations have gained attention due to their excellent compatibility with the existing Si-processing technology.[110,111] Regarding Si QDs embedded in SiN$_X$ matrix grown by PECVD using SiH$_4$ and N$_2$ and/or NH$_3$ mixtures, it has been found that when QDs surfaces are well passivated with Si—N and Si—H bonds, the samples have intense PL emission in the visible region.[112–114]

As shown in **Figure 10**a, it was reported that the correlation between the bandgap energy and the Si QDs size could be fit in accordance with the quantum confinement model, with constant $C = 13.9$ eV nm^2 for QDs embedded in silicon nitride films. This indicates that quantum confinement is remarkably increased in Si QDs spontaneously grown in silicon nitride films using SiH$_4$ and NH$_3$ mixtures in the PECVD system. The fitted bulk bandgap energy of 1.13 eV and the significant quantum confinement parameter of 13.9 can be attributed to an enhanced crystallinity and a well-passivated surface of Si QDs, as observed in Figure 10b. As discussed previously, PL emission mechanisms are strongly influenced not only by the structure (amorphous or crystalline), average size, dispersion, and density of Si QDs but also by their surroundings, which have a significant influence over the passivation of QDs surface and the chemical stability provided by the host matrix. It further depends on

the deposition method and preparation conditions, as shown in Figure 10c, where it can be observed that PL emission is changed as a function of the matrix compositions and annealing type.[115,116] On the other hand, Benami et al. reported the PL from Si nanoclusters embedded in SiN$_x$ films prepared by the PECVD technique from chlorinated precursors such as SiCl$_4$/NH$_3$/H$_2$ or SiH$_2$Cl$_2$/NH$_3$/H$_2$ mixtures. This work investigated the influence of hydrogen dilution on the structure, optical and luminescent properties of films and its impact on the PL characteristics in terms of the quantum confinement model. It was concluded that the PL peak position of the as-grown samples depends strongly on the H$_2$ flow rate and can be attributed to quantum confinement, whereas the intensity depends on the passivation state of the Si NCs embedded in the SiNx matrix, as presented in Figure 10d.[117] Goncharova et al. reported that the maximum PL emission strongly depends on the film stoichiometry, and it does not change significantly with different annealing temperatures and times (Figure 10e).[118] However, A. L. Muñoz-Rosas et al. reported electroluminescence (EL) of four configurations of metal–insulator–semiconductor (MIS)-type nanolayered structures, employing Si QDs embedded in silicon nitride luminescent films and dielectric silicon nitride (as a spacer). The average size and superficial density

ADVANCED
SCIENCE NEWS
www.advancedsciencenews.com

ADVANCED
PHOTONICS
RESEARCH
Open Access
www.adpr-journal.com

Figure 10. a) PL peak energy for crystalline Si QDs as a function of dot size. Dotted lines are fitted curves for crystalline Si QDs. The filled circles are data points obtained for Si QDs. b) TEM images of different samples show the Si QDs embedded in a silicon nitride film matrix to measure Si QD size. Reproduced with permission.[239] Copyright 2006, AIP Publishing. c) Room-temperature PL spectra of as-grown and annealed samples growth in different matrices. The insets show the corresponding emission color of the PL spot, as they are seen with the naked eye. Reproduced with permission.[115] Copyright 2006, AIP Publishing. d) Room-temperature PL spectra of silicon nanocluster for as-grown samples deposited at different H_2 flow rates. Reproduced with permission.[117] Copyright 2007, Elsevier. e) Representative PL spectra for the set of silicon nitride samples.[118] Copyright 2015, AIP Publishing. f) HRTEM images of SiQDs films.[119] Copyright 2018, MDPI.

**ADVANCED
SCIENCE NEWS**

www.advancedsciencenews.com

**ADVANCED
PHOTONICS
RESEARCH**

www.adpr-journal.com

for NPs were 3.1 nm and 6.04×10^{12} particles cm^{-2}, respectively (Figure 10f).[119]

Additionally, significant investigations have explored the use of chlorinated precursors (dichlorosilane, among others) and their influence on the microstructure, chemical stability, and PL properties of NPs and QDs in nitride matrices. The hydrogen from the precursor helps to extract the Cl from the thin-film surface, thus forming an HCl bond.[24] These reaction changes could be either exothermic or endothermic in nature. On the other hand, the probability that atomic hydrogen breaks the weaker bonds from the thin film, either on the surface or in bulk, is very high. Furthermore, depending on the energy attained, these bonds could be formed on the surface or in bulk due to the different reactions with the atomic hydrogen and dichlorosilane, generating silylene species anchoring in free dangling bonds. In these cases, the total concentration of hydrogen in the chamber is not only from H_2 but also from the NH_3 source. The most probable bonds to be broken during the reaction process are Si—H, N—H, and Si—Si.[24] In this way, the Si—H and Si—Si breaking bonds help in the formation of reaction centers for growth enhancement of Si NPs and QDs inside the SiNx matrix, whereas dissociation of the N—H bond endorses the matrix growth, favoring insertion of the silylene species (exothermic reactions) which can increase the average size of Si NPs and QDs. According to the theoretical calculations obtained in this report, in all cases, the insertion of silylene species on the Si—Cl and Si—H bonds generated crystalline zones in the nitride matrix producing many Si—Si bonds.[24] Consequently, the exothermic reactions could induce a local heating process inside the matrix, and as a result, the crystallinity of Si QDs is enhanced in the case of the SiN_x rich in Si, as evidenced by **Figure 11**a,b and the SAED images shown in Figure 11c when compared with Figure 11d–f for SiN_x matrix rich in nitrogen.[24] In all cases, these samples showed visible PL following the QCE, as observed in Figure 11g for the silicon-rich and nitrogen-rich matrix, respectively. It can be concluded, in this case, that by controlling the reaction phases and N/Si contents in nitride matrices, PL properties (peak positions and intensities) could be well-controlled to be used for desirable bioimaging applications.

6. Emission Mechanisms of Si Nanostructures in the Carbide-Related Matrix

After a brief discussion on essential aspects of oxide and nitride matrices, this section provides insights into carbide matrices. Silicon carbide (SiC) and oxycarbide (SiO_xC_y) thin films can play a crucial role in Si-based optoelectronic and photonic devices.[29,120–123] Silicon oxycarbide (SiO_xC_y) denotes the structure where Si is simultaneously bound to oxygen and carbon. It is considered a hybrid-nature material that owns the attributes of organic and inorganic functional groups.[124,125] Notably, its mechanical strength, thermal stability, and chemical properties depend on the inorganic part, whereas hydrophobicity, plasticity, and solubility depend on the material's organic components.[125–127] Moreover, the film features of the SiO_xC_y matrix strongly depend on the composition of multielements, that is, SiO_2 and SiC, etc. Hence, the property of SiO_xC_y thin film can be tailored by regulating deposition parameters.[127–129] Different
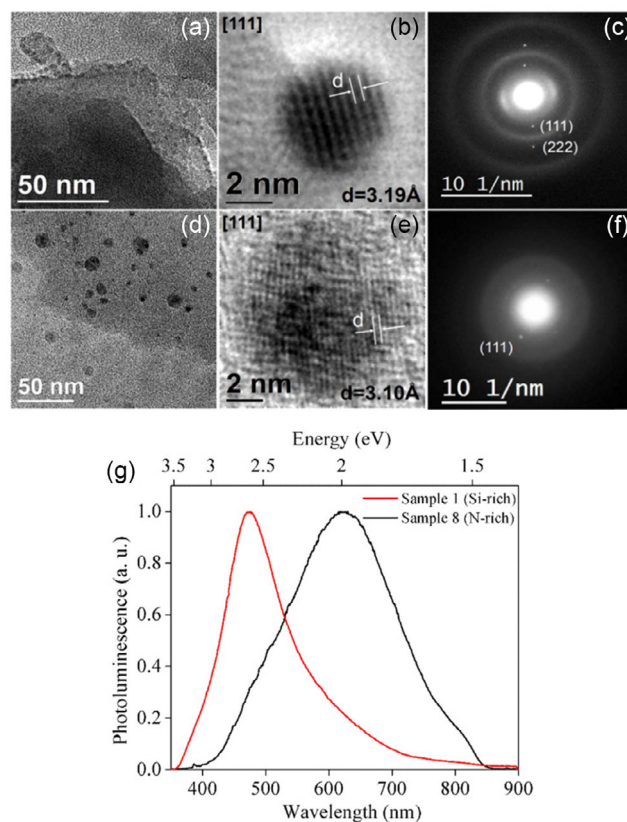
Figure 11. TEM micrograph of Si NCs embedded in the SiNx matrix. a) Samples growth in a condition to generate Si-rich matrix and d) samples opposite conditions to generate N-rich matrix. b,e) Zoom from Si nanocrystal images (a) and (d), respectively. c,f) SAED of images (b) and (e), respectively, presenting the orientation of the crystalline planes in Si NCs. g) Visible PL spectra of Si-rich (sample 1) and N-rich (sample 8) films when excited with a He–Cd laser at room temperature. Reproduced with permission.[24] Copyright 2016, IOP Publishing.

research groups demonstrate that carbide and oxycarbide matrices provide many more attractive features than conventional matrices.[22,28,29,120,121,130–132] Diverse research groups have also explored various applications of SiO_xC_y thin films in the biomedical field, as radiation-tolerant material, gas barrier coating for PET bottles, anode material for storage batteries, and piezoresistive sensors, among others.[133–143]

It is possible to regulate the refractive index between 3.2 and 1.5, respectively, by changing the oxygen–carbon ratio in this matrix.[144] This property has been used to develop low-loss waveguides in the near-infrared region.[145,146] Conversely, in recent years, the PL study on SiO_xC_y thin films has increased prominence due to its wide range of intensive emission in the visible spectra in recent years.[29,120–123] **Table 3** summarizes different methods for obtaining Si QDs embedded in the carbide and oxycarbide matrices and some of their related properties.

6.1. PL Mechanisms

The PL origin has been investigated by various authors so far using different characterization techniques such as X-ray

Table 3. SiO_xC_y matrix: preparation methods, precursors, PL emission band, and related mechanisms of PL emission.

Synthesis method	Precursors	PL [eV]	Properties	References
Radio frequency (RF) sputtering	SiO_2 + C plates	2.2	Carbon clusters ($\approx$2 nm) comparable or smaller than C_{60}	[147,148]
Magnetron co-sputtering	Suprasil + Graphite chips	1.8–2.2	C-related defects, a-Si:O:C regions, and carbon clusters in a-SiO_2:C	[260]
I-Imp[a]	SiO_2 + Si^+ + C^+	1.4–1.6, 2.0–2.2 and 2.7	Formation of silicon nanocrystals (1.4–1.6 eV), carbon amorphous clusters (2.0–2.2 eV), and SiC clustering (2.7 eV)	[149–151]
I-Imp[a]	SiO_2 + Si^+ + C^+	1.9, 2.5, and 2.7	Formation of Si NCs (1.9 eV), SiC and/or a complex of Si, O, and C (2.5 and 2.7 eV)	[152]
I-Imp[a]	SiO_2 + C^+	2.53	Amorphous carbon clusters	[261]
I-Imp[a]	SiO_2 + Si^+ + C^+	2.1 and 2.7	Amorphous carbon clusters (2.1 eV) and $Si_yC_{1-y}O_x$ complexes ($x < 2$) (2.7 eV)	[153]
RF co-sputtering	SiO_2 + C plates	2.27, 2.54	C-rich clusters (2.27 eV) and SiC NCs luminescence centers (2.54 eV)	[164]
RF co-sputtering	SiO_2 + SiC	2.7	Defects in SiO_2 at the SiC/SiO_2 interface: Two-fold coordinated silicon defect (i.e., O–Si–C–O– and –O–Si–O–) and Neutral oxygen vacancy (NOV) defect	[156]
ECR PECVD[b]	SiH_4 + O_2 + CH_4	2.46	Carbon-incorporated Si nanoclusters	[165]
Thermal carbonization/ oxidation of porous silicon	Porous Si + (N_2/C_2H_2) + wet argon	2.5	Carbon bonding state and Carbon-based clusters in a silicon oxide matrix	[262–266]
Pyrolysis process by sol–gel method	SiO_2 + triethoxysilane and methyldiethoxysilane	2 and 2.21	The presence of a low amount of free C and SiC (2.21 eV) and presence of Si, C and SiC in the film (2 eV)	[43]
Atmospheric pressure VHF microplasma jet	TEOS-Ar	2.7	NOV defects	[267]
TCVD[c]	2,4,6-trimethyl-2,4,6-trisila-heptane ($C_7H_{22}Si_3$) + O_2	2.13	CODCs and electronic transitions of Si—C/Si—O—C bond	[122,157]
RF magnetron sputtering	SiC + O_2 + Ar	2.64, 3.22 and 3.78	The ODCs (3.78 eV), Si-O_x related defects (3.22 eV) and surface defects of 6H SiC nano-crystal particles (2.64 eV)	[128,268]
Catalyst-assisted process	SiO_2 + CH_4	2.34 and 3.26	ODC in SiO_2 shell (3.26 eV) and QCE in β-SiC nanowires (2.34 eV)	[269,270]
VHF-PECVD	SiH_4 + CH_4 + O_2	1.68. 2.13 and 2.7	Si-related NOV Defect (2.7 eV), Si–C related defect state (2.13 eV) and silicon dangling bond (DB) defects (1.68 eV)	[158-160]
Molten salt mediated carbothermal reduction route	Silica fume and sucrose	2.93	Quantum size effect due to SiC NWs	[271]
HWCVD[d]	Monomethyl-silane (MMS) + O_2	2.21, 2.7 and 2.95	Combination of different defects and QCEs in the SiOC matrix	[28,121,132]
Cat-CVD[e]	TEOS + Ar	2.48, 2.21, 2.7 and 2.95 − 3.26	Formation of Si and SiC-based nano-crystals (2.48 and 2.21 eV) and Defects with H and C related bonds and ODC defects (3.26–2.95 and 2.7 eV)	[22,29,121,272]
HFCVD[f]	Ethanol + SiO_2 + H_2	2.7–2.8	Si related defects such NOVs and ODCs	[123]
RF magnetron sputtering	Si or SiC target + O_2 + CH_4 + Ar	2.5	Formation of light-emitting centers in SiO_x and amorphous carbon nanoclusters	[120,273]
Cat-CVD[e]	Mesoporous silica pellets and TEOS	2.95–3.26	QCEs due to Si—C/Si—O—C bonding groups	[274]
Chemical treatment	Fumed silica + Tetramethoxysilane [$Si(OCH_3)_4$]	2.5	Carbon precipitates (nanodots)	[275]

[a] Ion-Implantation; [b] Electron Cyclotron Resonance-PECVD; [c] Thermal chemical vapor deposition; [d] Hot-wire Chemical Vapor Deposition; [e] O-CAT CVD; [f] Hot filament chemical vapor deposition technique.

diffraction (XRD), high-resolution transmission electron microscopy (HRTEM), electron paramagnetic resonance (EPR), and TRPL. The role of NPs size in describing the PL mechanisms of the SiO_xC_y matrix was first explained by Hayashi et al., where

the role of carbon clusters in the SiO_xC_y matrix was discussed, concluding that carbon clusters ($\approx$2 nm), equal to or smaller than C60, could influence PL in the 2.2 eV band.[147,148] B. Garrido et al. also described the role of QDs in SiO_2 implanted with

carbon and Si and explained the reason for PL at different bands such as 1.4–1.6, 2–2.2, and 2.7 eV, due to the formation of QDs (1.4–1.6 eV), amorphous carbon clusters (2-2.2 eV), and SiC clustering (2.7 eV), respectively.[149–151] Moreover, other authors suggested as well that the formation of NCs, amorphous carbon clusters, SiC, and/or a complex of Si, O, and C such as $Si_yC_{1-y}O_x$ complexes ($x < 2$) could exert influence for PL at 1.9, 2.1, and 2.7 eV bands, respectively.[152,153] The formation of these SiC NPs and QDs is crucial for modern-diagnostic imaging devices, and more information can be found in Section 7.

Theoretically, the confinement effect of SiC can be illustrated using Equation (10) supporting the relation between calculated PL peak energy emission and QDs size, as an example, 1–3.42, 3–2.09, 5–1.79 eV.[29,154] Here, it is worthwhile to mention that the theoretical explanation for the effect of Si NPs is already

discussed in the previous section. Additionally, **Figure 12**a–g shows the TEM image of an amorphous SiO_xC_y matrix showing the random distribution of SiC and Si QDs in this matrix.

$$E = 1.24 + \frac{2.18}{d^{0.850}} \qquad (10)$$

Furthermore, different defect-related mechanisms have also proposed the explanation of PL in the SiO_xC_y matrix. For example, Kontkiewicz et al. suggested that the blue PL band in porous silicon (p-Si) was related to the defects in SiO_2 due to carbon impurities.[155]

Guo et al. explained the blue–green luminescence by the formation of defects like twofold coordinated Si, for example, $-O-Si-C-O-$ and $-O-Si-O-$ and neutral oxygen vacancy
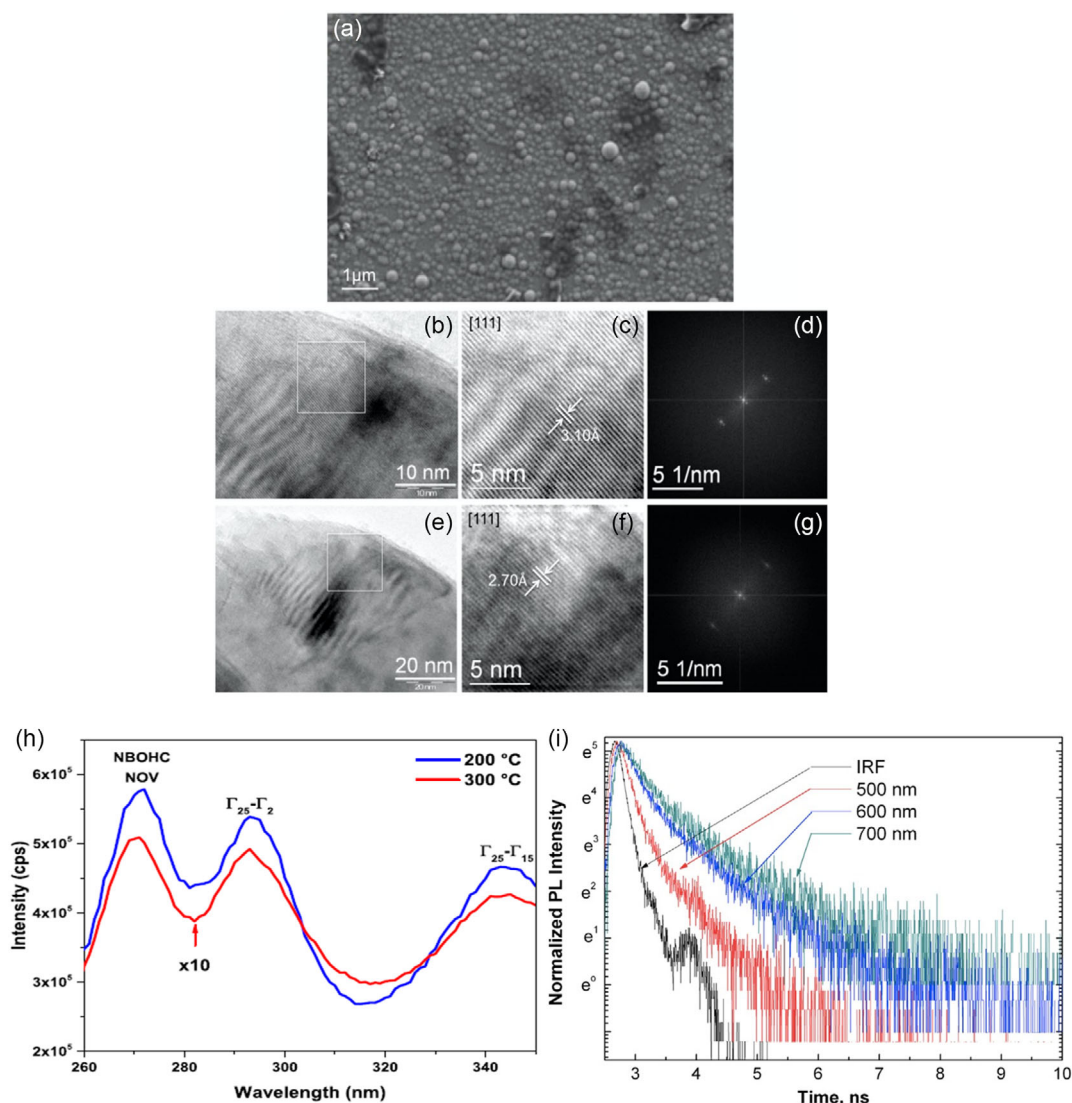
Figure 12. Distribution of Si and SiC NPs in SiO_xC_y matrix. a) scanning electron microscopy (SEM) image of thin film; b–d) TEM images correspond to Si NPs; e–g) TEM images refer to SiC NPs. Reproduced with permission.[29] Copyright 2019, Elsevier. h) PLE spectra of SiO_xC_y matrix. Reproduced with permission.[28] Copyright 2019, Elsevier. i) PL decay curves of emission normalized on the intensity of laser pulse at 500, 600, 700 nm excited by 405 nm.[120] Copyright 2017, Elsevier.

(NOV) defect at the interface of silicon carbide (Si−C) QDs and SiO$_2$ matrix.[156] Later, some authors assigned the PL band at 1.68 and 2.7 eV due to Si dangling bond (DB) defects and Si-related NOV defects, respectively. In contrast, Si−C-related defect state and CODCs were assigned to the 2.13 eV PL emission band.[122,157–160] Besides these reports, Ramos–Serrano et al. tried to explain the PL due to the combination of different defects mechanisms, for example, NBOHC, NOV, among others, and QCEs in the matrix of SiO$_x$C$_y$ PL excitation (PLE) spectra and TRPL characterizations.[28] Though, the main contribution was found to be originated from the confinement phenomena. The PLE is shown in Figure 12h, where excitation bands can be observable at different peaks, i.e., 265, 295, and 345 nm, respectively. Here, the presence of the excitation band at 265 nm can be referred to as NBOHC and NOV defect centers, which are related to the luminescence at 450 nm and 610–650 nm bands, respectively.[161] Besides, other excitation bands are observed at 295 and 345 nm, which are very close to the direct optical transitions in bulk Si, that is, (Γ_{25}–Γ_{15}) and (Γ_{25}–$\Gamma_{2'}$) absorption transitions at 295 and 365 nm, respectively.[162] The shift in the (Γ_{25}–$\Gamma_{2'}$) absorption transitions from its bulk Si value and the presence of another excitation band at 295 nm can be referred to as the origin of PL due to QCE.[28,163]

A.V. Vasin et al. reported that characteristic decay time depends on the emission energy and decreases significantly with increasing the emission energy (Figure 12i).[120]

The annealing process is also worth discussing, which helps us to distinguish the origin of PL between defects-related mechanisms and the QCE of NPS and QDs embedded in the SiO$_x$C$_y$ matrix. If the PL band shifts after the terminal annealing process, it indicates that the size of C clusters or NPs and QDs changes, which in turn changes the position of the PL band. On the other hand, PL does not shift with the increasing annealing temperature due to defect-related luminescence centers.[156,164]

6.2. Si/C/O Ratio and their Influence on PL

The silicon, carbon, and oxygen ratio in the SiO$_x$C$_y$ matrix play an important role, and it may contribute to explain the influence of these elements on PL emission. Several authors have discussed the effect of C and Si in thin films.[122,123,153,165,166] The impact of carbon on the PL and fourier transformed infrared (FTIR) spectra, including the bond area ratio of (Si–C)/(Si–O), is shown in **Figure 13** based on previous studies.[122,123,166] In Figure 13a, the influence of different C content on the rocking and stretching modes for the Si−O−Si bonding is shown at 470 and
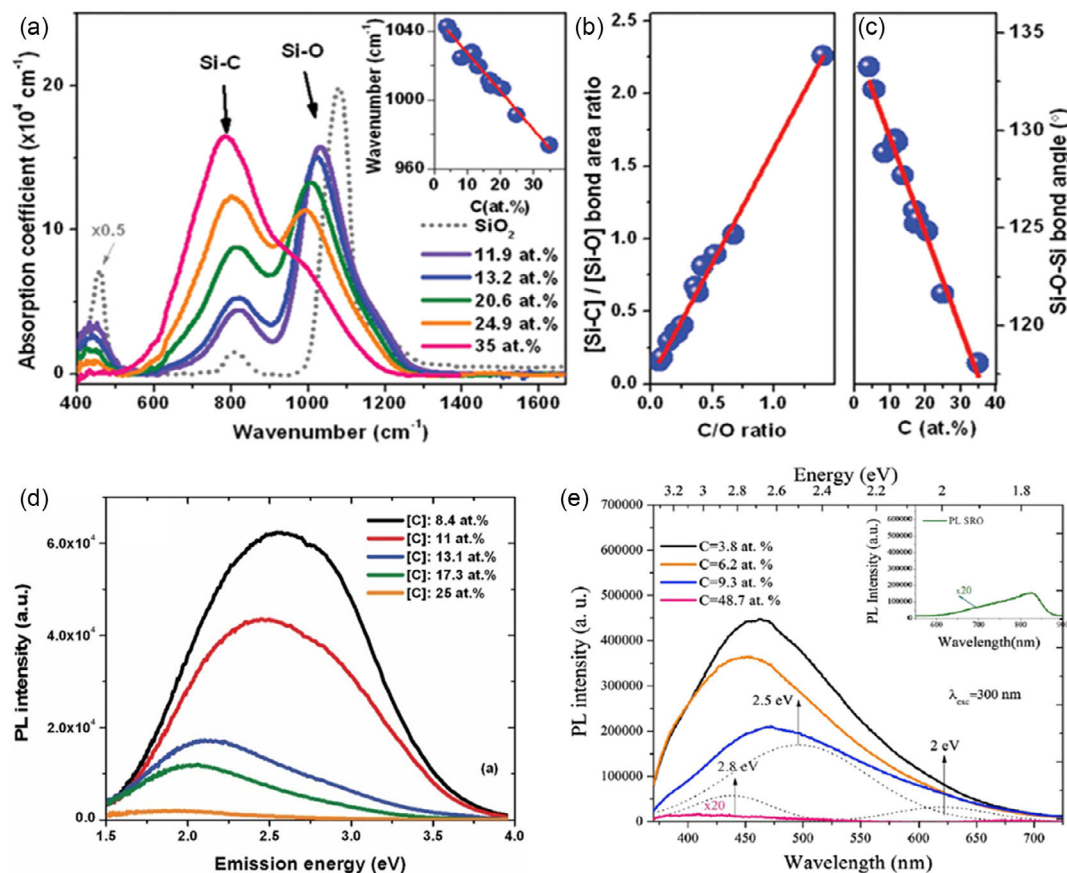
Figure 13. a) FTIR spectra of SiO$_x$C$_y$ matrix for different C contents. The inset illustrates the shift in the Si–O stretching bond as a function of C content. b) The effect of C/O on the bond area ratio of (Si–C)/(Si–O). c) The effect of C content on Si–O–Si bond angle. Reproduced with permission.[166] Copyright 2017, IntechOpen. d,e) PLE spectra of SiC$_x$O$_y$ films with different carbon concentrations. Reproduced with permission.[122,123] Copyright 2014, AIP Publishing and Copyright 2020, Elsevier.

**ADVANCED
SCIENCE NEWS**

www.advancedsciencenews.com

**ADVANCED
PHOTONICS
RESEARCH**

www.adpr-journal.com

$1080 \, cm^{-1}$, respectively, while the position of the Si—C bond is localized at $800 \, cm^{-1}$.[132] The blueshift of these Si—O—Si bands in the FTIR spectra can be observable with the increment of %C in the SiO_xC_y matrix, while the abetment of Si—O—Si bondings represent the nature of the film, shifting from SiO_2 to SiC. Moreover, Figure 13b shows the linear increase of the bonding area ratio of (Si—C)/(Si—O) demonstrated with the proportional content of the C/O ratio. In contrast, Figure 13c shows the effect of C content on the Si—O—Si bond angle.

The shift in the Si—O—Si stretching bond can also be referred to as oxygen deficiency, which may increase the possibility of carbon and/or neighboring silicon atoms with the Si—O—Si bond, which could help in tuning the PL spectra and its intensity.[120,132,167–169] Gallis et al. and Coyopol et al. described the effect of %C on PL spectra, as shown in Figure 13d–e.[122,123] In both figures, it is easily observed that the intensity of PL spectra decreases with respect to the C increment in the SiO_xC_y matrix while the spectrum shifts from blue to red. Therefore, it can be concluded that the amount of carbon content may help to tailor the PL properties of the SiO_xC_y matrix. In summary, the strong white light emitted by SiO_xC_y is a sum-up of factors such as the confinement effect (similar to those of oxide thin films) and other characteristics closely related to the density of Si—O—C bonds, with the oxygen defect centers attached to the carbon.[157] The effect of C content is also discussed for PL spectra, where it is observed that the low carbon content in the SiO_xC_y matrix shows a better PL response.

After reviewing the structural, morphological, and optoelectronic features of oxide, nitride, and carbide matrices, the next section will deal with the application of these matrices in biological applications. Significantly, the discussion mentioned in the earlier sections on the luminescence mechanisms of NPs and QDs embedded in these matrices will help to design stable, controllable, efficient bioimaging and biosensing systems. A piece of complete knowledge of the properties and emission mechanisms will allow experts from multidisciplinary areas to come forward and work on the development of modern detection systems with desired characteristics.

7. Silicon-Based Matrices and Optical Properties: A Viewpoint for their Application in Biological Systems

Nanomaterials research for biological applications has an actual emerging projection and beyond. The use of specific nondestructive techniques, such as PL, from Si-based compound thin films has opened a new pathway for developing novel nanomaterials compatible with biological systems (bacteria, yeast, animal cells, and tissues).[170] Nevertheless, depending on the characteristics offered by each Si matrix (size, porosity, toxicity, emission mechanisms, biocompatibility, chemical stability, and target affinity), these can be focused on applications for the identification of target analytes either inside or outside the biological systems. For instance, Si nanomaterials with high biocompatibility and low cytotoxicity can be employed in applications in the clinical sector. Si NCs and their composites have an important projection in the biological field, which contain almost no heavy metals or less toxic metals. As far as the authors know, silicon by

itself can be degraded into nontoxic silicic acid in vivo and excreted in the urine and stool.[171] In some cases, biocompatibility is also explored through the fusion with another material with a perspective of polymer encapsulated. Shiohara et al. reported that the biostability (no cytotoxicity) of epoxide-terminated Si QDs is maintained until $112 \, \mu g \, mL^{-1}$ in vivo, whereas diol-terminated Si QDs were biostable until $448 \, \mu g \, mL^{-1}$.[172] Erogbogbo et al. studied polyethylene glycol (PEG) micelle-encapsulated Si QDs as fluorescent probes used for in vivo imaging, finding that the inhibitory particle concentration was higher than $500 \, \mu g \, mL^{-1}$, corresponding to 50% cell viability.[173] In addition, Ya-Kun Dou studied water-dispersible Mn^{2+}-functionalized Si NPs, which maintained stability at different pH and NaCl solutions showing excellent biocompatibility.[174] On the other hand, nanomaterials with specific features that could compromise cellular functions can be used to detect analytes immersed in external environments. In this sense, Si-based nanomaterials have a projection for broad-field applications in cell imaging, drug release, biomarking, immunotherapy, and biodetection, among others. Besides, QDs are robust nanostructures that enhance these interactions through their size, improving PL features, even advantageously over traditional dye molecules or fluorescent proteins.[175] The applications are diverse, and as stated before, a specific size configuration allows distinctive characteristics that could be improved with embedded Si QDs. This section will discuss studies focused on the versatility and contribution of Si-based nanomaterials that provide optical responses (PL, fluorescence, Raman) and their application in the biological sector **(Figure 14)**.
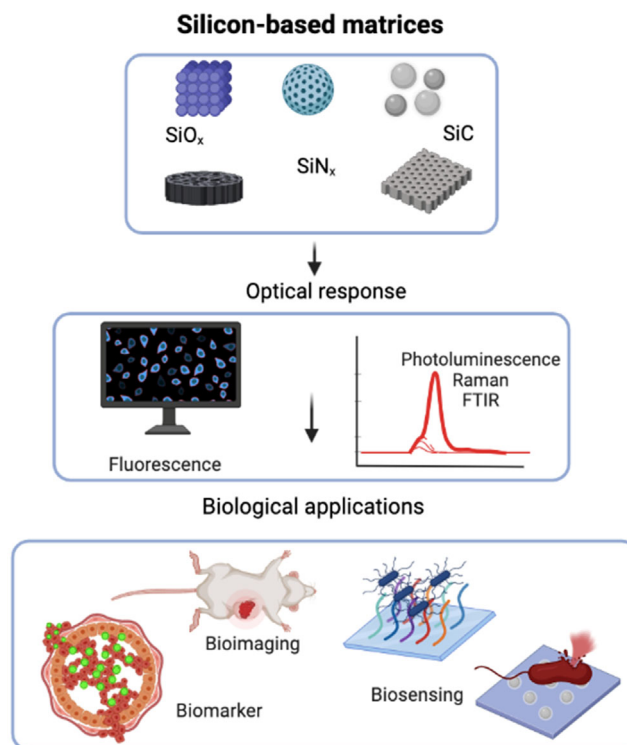
Figure 14. General overview of biological applications of Si-based nanomaterials (Created with BioRender.com).

7.1. Interaction of Silicon-Based Nanomaterials with Live Cells: A Perspective for the Clinical Sector

Since Si is an element commonly found in traces and excreted from the organism through the urine; their NPs can represent an alternative to materials based on toxic heavy metals in biological surroundings.[176,177] Likewise, the main concerns regarding the use of these technologies are the biodegradability and toxicity of the nanomaterials themselves.[178–180] In clinical applications for humans, renal clearance can mitigate toxicity; however, it can maintain harmful components in mononuclear phagocytic system (MPS) organs.[170,181] The required hydrodynamic size for renal clearance is <5.5 nm.[181] Therefore, the Si NPs' size improvement, matrix configuration, and biocompatibility will determine their application in the biotechnological field. In **Table 4**, we present diverse works about nanostructured Si-based materials (SiC, SiO$_x$, and SiN$_x$) and their interactions with animal cells that have found application in bioimaging, biolabeling, drug release, cell therapy, and osteointegration.

Carbide matrices have unique electrical, mechanical, and thermal properties, which can be implemented for on-chip integration applications (microdevice) through thin-film 3C-SiC MEMs with a specific function.[29] Moreover, SiC NPs can carry good PL at lower wavelengths than Si NPs alone, which is considered a

Table 4. Silicon-Based nanomaterials for clinical applications.

Silicon compound	Matrix	Response	Analyte studied	Biological application	References
SiC	3C-SiC QDs NPs < 1.6 nm	PL Fluorescence	3T3-L1 fibroblasts	Bioimaging	[276]
	SiC QDs embedded on nano-Ag/SiN$_x$/glass substrates	PL	3T3-L1 fibroblasts	Bioimaging	[277]
	Si QDs/Au core–shell nanostructures	Fluorescence	Pancreatic cancer cells (Panc-1, MIA PaCa-2 and ASPC-1)	Bioimaging	[278]
	Ultrathin epitaxial deposited SiC membranes	Fluorescence	Mouse 3T3 fibroblast	Bioimaging	[183]
	Ultrasmall SiC USNPs < 3 nm	Fluorescence	BSA[f]	Biomarker	[279]
	SiC NPs < 5 nm	Fluorescence	3T3-L1 murine fibro- blasts, HSC-2[g] and S-G (human immortalized gingival epithelioid) cell lines	Biomarker	[188]
	Nitrogen-doped 3C-SiC[a] over PDMS[b] substrates connected via graphite layer	Raman measurements of PL (3C-SiC[a] characterization) Electrochemical measurements and I–V characteristics	Hearts from Adult rats	Electrical modulation on tissue activity	[185]
	Ultrasmall SiC NPs with different termination groups (SiC–x, SiC–NH$_2$, SiC–OH)	Flow cytometry	SAOS-2[h] and human monocytic/macrophage cell line (THP-1)	Immune cell therapy (stimulatory effect of NPs)	[204]
	SiC and core/shell SiC/SiO$_x$ nanowires	Fluorescence	MC3T3-E1 pre-osteoblastic cells	Osteoblast adhesion	[186]
SiO$_x$	LPSiNPs[c]	PL	Tumor in mice and MDA-MB-435 human carcinoma cells	Imaging and drug loading	[280]
	MSNPs[d]	NIR[e] fluorescence	Tumor treatment in vivo, a human sarcoma cell line (HT-1080)	Drug release	[281]
	Si-NPs	PL, Fluorescence	N/A	Bioimaging	[282]
	Si QDs	PL	Fibroblast cell lines A549 and L929	Bioimaging	[283]
	SiO$_2$ QDs	PL	Cancer cells	Bioimaging	[6]
	Si-NPs optically active defect centers using tetraethyl orthosilicate	PL, Fluorescence	Mouse hepatocytes (FL83B), human carcinoma (A549), and murine macrophages (Raw 264.7)	Bioimaging	[189]
	NaYF$_4$ NPs coated with SiO$_2$ shell (NaYF$_4$:20%Yb, 0.2%Tm@SiO$_2$)	Luminescence (NPs characterization) NIR and UV light	Mammalian cancer cell line 4T1	Photodynamic cancer cells therapy	[194]
SiN$_x$	Si$_3$N$_4$ substrate disks	Raman spectroscopy	SaOS-2[i]	Osteo-integration for bone repair devices	[195]
	Sandblasting Si$_3$N$_4$ substrates	Raman spectroscopy and Fluorescence	SaOS-2[i]	Osteo-integration and production of bone tissue	[284]

[a]Cubic silicon carbide; [b]Polydimethylsiloxane; [c]Luminescent porous Si NPs; [d]Mesoporous silica NPs; [e]Near-infrared; [f]Bovine serum albumin; [g]human oral squamous carcinoma; [h]Human osteoblastic cell line; [i]Human osteosarcoma cell line;

promising composite material for optoelectronic devices. Regarding fabrication, it is possible to deposit SiC using a safe and inexpensive precursor at a relatively low temperature, around 300 °C.[29,182] For instance, Nguyen et al. fabricated SiC ultrathin membranes (50–150 nm) to be applied as cell growth substrates compatible with bio-MEMs platforms to enable studies of cell stretching and mechanotransduction, where they found high rates of cell viability (92.7% up to 72 h).[183] Another work about polycrystalline SiC thin-film deposition (700 nm) was performed by Diaz-Botia et al. in an electrode array to record nerve responses of electrical stimulations that could be applied for long-term chronic implantable electrodes.[184] An improvement to this application concept was implemented by Nair et al. using 2D and 3D printing of 3C-SiC over polydimethylsiloxane (PDMS) substrates, also applied to tissue modulation activity, taking advantage of the material properties such as pseudocapacitive electrochemical behavior and photoelectrochemical activity.[185] Another recent approach in biomedicine involves using composite nanowires (SiC/SiO$_x$) with a hydrogen plasma

treatment to promote osteoblast adhesion and spreading for bone tissue engineering.[186] On the other hand, SiC and SiC-based composite nanostructures have been used to fabricate nanowires (1D), NPs, and QDs (0D). SiC-based NPs are mainly used in bioimaging for cell monitoring, assessing non-toxicity, and suitability for biological interaction, as can be observed in Table 4. Regarding some specific configurations, such as QDs, these fluorescence properties have been improved due to their interesting properties derived from their size and characteristic narrow emission spectra that can offer higher fluorescent signals even measured from a single cell.[187] This has great potential in the clinical sector, as observed by the work of Serdiuk et al., who employed SiC NPs as nanoprobes to discriminate between healthy and carcinogenic cells, taking advantage of the material size to enhance the SiC NPs' intracellular uptake and localization to make a correlation with cell proliferation.[188] A higher NP uptake was observed in cancer than in healthy cells as cellular division increased, with a particular affinity of NPs to the nucleus **(Figure 15**a,b).
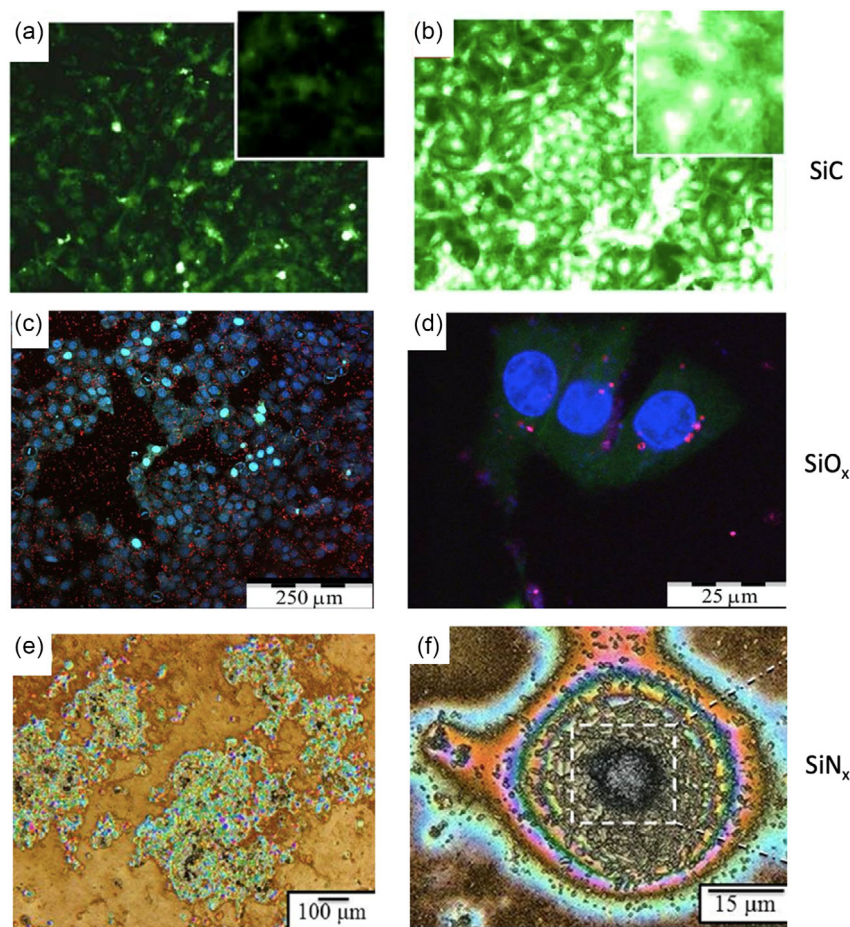
Figure 15. Si-based materials used for biomedical applications. a,b) Fluorescence microscopy images of SG cells labeled by SiC NPs at the total confluence. In healthy SG cells (a), the labeling is low and absent in the nuclei at a low confluence, increasing when cells divide, suggesting that labeling depends on the state of confluence. In cancer cells (b), intracellular luminosity levels are high and independent of confluence. Reproduced with permission.[188] Copyright 2012, Wiley-VCH. c,d) Fluorescence microscopy images of CF2Th cancer cells incubated with LA-Si NPs (observed red and pink colored) under two magnification scales. Reproduced under the terms of a Creative Commons Attribution CC-BY License.[6] Copyright 2016, The Authors, published by Springer Nature. e,f) Laser-scanning micro- graphs of the osteosarcoma cells in situ during apatite formation. The early exposure to Si$_3$N$_4$ substrate is followed by hydroxyapatite formation at a later stage. Reproduced with permission.[195] Copyright 2016, ACS Publications.

Similarly, silicon dioxide (SiO$_2$) NPs have been mainly employed in bioimaging applications at different cell lines, as shown by Yoo et al.[189] They verified the lack of SiO$_2$ NPs' cytotoxic effects on FL83B (mouse liver), A549 (human lung cancer), and Raw 264.7 (macrophage) cells assessing their biocompatibility. Additionally, SiO$_2$ NPs have shown increased applicability in drug delivery systems in carcinogenic cells, exploiting the material porosity. For instance, host matrices of Si and porous SiO$_2$ have been used in in vitro release of the steroid dexamethasone, ibuprofen, cis-platin, and doxorubicin, proposed to treat different cancer types.[190–193] However, the enhancement of PL responses by QDs has not been completely studied in SiO$_2$ NPs. The last work related to SiO$_2$ QDs confirmed their biostability for several days, since there were observed characteristic differences in cell proliferation states as well as NPs localization (Figure 15c,d).[6] A recent application focused on using a hybrid nanomaterial NaYF$_4$:20%Yb,0.2%Tm@SiO$_2$, allowing reactive oxygen species (ROS) generation after NIR excitation, with detrimental effects on mouse's mammary gland cell lines, with a possible application in targeted cancer treatment.[194] Lastly, silicon nitride has been mainly used for osteointegration experiments with potential application in bone tissue repair, as observed by Pezzotti et al. (Figure 15e,f).[195] As far as the authors know, a few works related to QDs integration in SiN$_x$ substrates are still unexplored and represent a further research opportunity in this area.

In summary, the performance of Si QDs and NPs for biological applications must ensure biocompatibility, biostability, and also efficient PL response. He et al. reported O–Si NCs/antibody bioconjugates for cell imaging with double color. They showed that the Si NCs conjugated with HEK293T cells resulted in high PL quantum yield (PLQY) (25%).[196] In some cases, the luminescent properties of bioconjugates are a function of the surface interaction, and the quantum size effect has a minor impact.[197] Li et al. reported a complete characterization of surface nitrogen-capped Si NPs with PL quantum yield of up to 90% and narrow PL bandwidth of −40 nm. However, the surface of Si NPs was modified with different ligand types to observe that PL performance is comparable with commercial dyes and QDs.[198] These advances in the study of molecule interaction represent a milestone to focalize the efforts in understanding PL variations after bioconjugation to be better applied in biological systems.

7.2. Biosensing of Microorganisms

As mentioned earlier, apart from the clinical applications, Si-based nanomaterials have opened a new paradigm in the biosensing of the microorganisms such as *E. coli*, *Salmonella typhimurium*, *Porphyromonas gingivalis* and *Staphylococcus epidermis*, and other pathogens like rotavirus and *Candida albicans*. A summary of the latest reports in this field can be found in **Table 5**. For example, SiC has been used to develop biosensor devices using film configurations. Celis-Herrera et al. developed interdigitated microelectrode arrays that detect *E. coli* EPEC after 5 min incubation using an electrical response (impedance spectroscopy).[199] In this sense, using an amorphous substrate could benefit the biofunctionalization strategies, influencing the final sensitivity of biosensor devices.

With respect to SiO$_2$, Chitra K. and Annadurai G. reported the use of Si NPs (151–165 nm) as nanoprobes for the detection of pathogenic *E. coli* (**Figure 16**a,b).[200] They added amine-reactive dye to prepare fluorescent silica NPs, obtaining this fluorescent property after 24 h incubation. However, although a proficient

Table 5. Silicon-Based compound nanomaterials for microorganisms biosensing.

Silicon compound	Matrix	Response	Analyte studied	Biological application	References
SiC	Interdigitated microelectrode arrays of a-Si$_x$C$_{1−x}$:H	FTIR EIS[c]	*E. coli*	Biosensing	[199]
	a-SiC:H films	FTIR	*E. coli* DH5α	Biosensing	[285]
	a-SiC:H Thin Films	FTIR	*Salmonella Typhimurium*	Biosensing	[286]
SiO$_2$	Si-NPs	Fluorescence	*E. coli*	Biosensing	[200]
	Hollow silica nanospheres	Fluorescent responses	*E. coli* O157:H7	Biosensing	[287]
	SiO$_2$ layer of SiO$_2$ shell-coated Fe$_3$O$_4$ NPs	EIS[c]	Basophilic leukemia cell (RBL-2H3) cell	Biosensing	[288]
	SiO$_2$ chip SiO$_2$–Ag–SiO$_2$	SPR[d]	Stroke biomarkers: NT- proBNP and S100β	Biosensing	[289]
	SiO$_2$ and Si$_3$N$_4$ wafers	Fluorescence	Mouse γ-globulins	Biosensing	[290]
SiN$_x$	Si$_3$N$_4$/SiO$_2$ nanostructures	Fluorescence	BSA	Label-free biosensors	[291]
	QS[a] microstructures coated with a thin layer of Si$_3$N$_4$	PL	*E. coli*	Biosensing	[201]
	SiN microchips	Electron microscopy imaging	Rotavirus	Monitoring of viral surveillance	[292]
	Si$_3$N$_4$ bioceramics	Raman spectroscopy and fluorescence	*Porphyromonas gingivalis*	Biosensing, lytic activity	[202]
	Si$_3$N$_4$ substrates	Fluorescence, In situ Raman spectroscopy	*Staphylococcus epidermis*	Biosensing, lytic activity	[293]
	PMMA[b]/Si$_3$N$_4$ composites	Raman spectroscopy, Fluorescence	*Candida albicans*	Fungicidal action	[203]

[a]QS; [b]Polymethylmetacrylate; [c]Impedance spectrum; [d]Surface plasmon resonance.
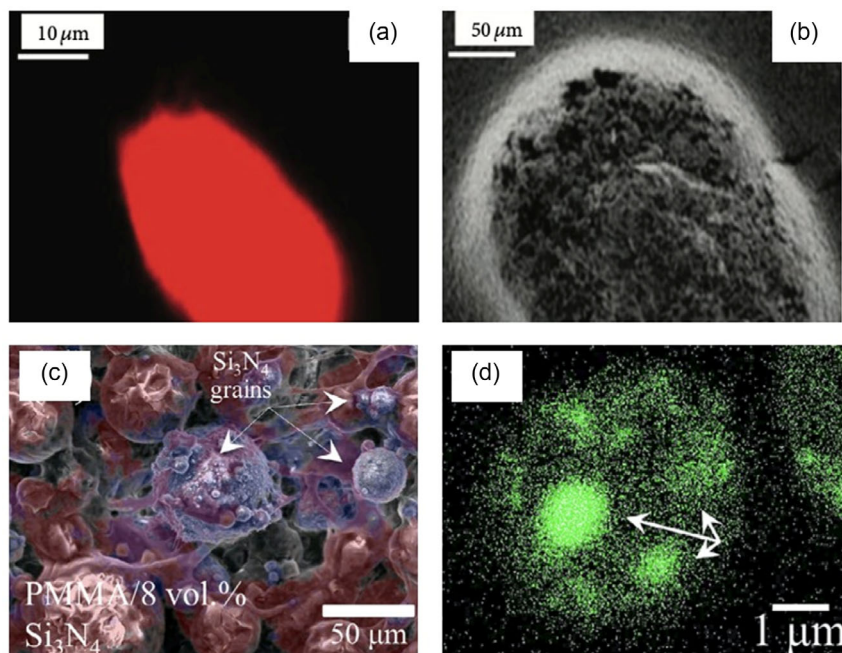
Figure 16. Si-based materials used for biotechnological applications. a) Fluorescence image of bacteria. b) SEM image of *E. coli* after incubation with antibody-conjugated Si NPs. Reproduced with permission.[200] Copyright 2013, Hindawi. c) Energy dispersive spectroscopy (EDS) analyses from SEM micrographs of PMMA/8 vol% Si_3N_4 substrates showing Si_3N_4 grains localization. d) Fluorescence image of *C. Albicans* incubated for 24 h to PMMA/8 vol% Si_3N_4 substrates. Arrows point at mitochondria-like roundish regions. Reproduced with permission.[203] Copyright 2021, Elsevier.

fluorescence signal was obtained, the limit of detection (LOD) was not shown through PL measurements. On the other hand, Duplan et al. developed quantum semiconductor (QS) microstructures enveloped with a Si_3N_4 layer, achieving an in situ detection of 104 CFU ml^{-1} *E. coli*.[201]

Finally, for the case of Si_3N_4 substrates, recent reports have demonstrated their lytic activity using this feature for pathogen recognition, providing an antimicrobial or fungicidal effect. This was observed by Pezzoti et al. in *Porphyromonas gingivalis* and *Candida albicans* (Figure 16c,d), showing an additional application for these kinds of substrates that can improve their applicability.[202,203] Since Si-based materials can be biofunctionalized to be platforms applied for biological detection through optical biosensors, using QDs in the different sensor surfaces could increase the biosensor sensitivity. By improving their optical properties (PL, fluorescence), the response interface could enhance the biosensing performance to detect the target analyte. This suggests a higher capacity to detect minimal changes in the PL values that can be correlated to lower concentrations, taking advantage of the fluorescence and photoluminescent emission of QDs. It is worth mentioning that there are just a few published works considering this perspective, and this opens a new paradigm of using these biocompatible materials for bioimaging applications.

As shown from a clinical applications perspective, the properties of Si-based compound nanomaterials have been mostly used for bioimaging and biomarkers because of their low toxicity and compatibility with biological interaction. Moreover, an enhanced response has been observed for integrated or composite materials from these nanostructures, as previously mentioned in the past sections for SiO_xC_y matrices, attributed to their organic and inorganic functional group composition. This has been demonstrated recently by the work of Bělinová et al. which probed ultrasmall SiC NPs with functional groups (SiC_x, $SiC–NH_2$, $SiC–OH$) in human monocytic /macrophage cell lines (THP-1) for immune cell therapy.[204] Similarly, Kowalik et al. used NaYF4 NPs coated with SiO_2 shells for application in photodynamic cancer cell therapy.[194] Undoubtedly, all these applications could be significantly improved by modulating the PL emission after understanding the mechanisms for real-time monitoring of bacteria (*E. coli*, *Porphyromonas gingivalis*, *Staphylococcus epidermis*), fungi (*Candida albicans*), rotavirus, cellular repair processes, and cancer treatment evaluation.

8. Conclusions and Future Perspectives

Despite the widespread literature published about Si nanostructures and their optical properties, to the best of our knowledge, there are almost no reviews focused on comparing the emission mechanisms of Si NPs and QDs in different matrices (SiO_x, SiN_x, and SiC), highlighting the suitable optoelectronic features of these materials. It has been discussed that the barrier height is also one of the deciding factors for optoelectronic properties. Lower barrier height in nitride and carbide matrices makes them better conductive than silicon oxide surrounding. At the same time, these matrices are proposed as alternatives due to their lower barrier height and higher mobility. Another prospect of applying these films is improving solar cell efficiency, using them as antireflective and downshift layers, which absorb UV

ADVANCED
SCIENCE NEWS
www.advancedsciencenews.com

ADVANCED
PHOTONICS
RESEARCH
Open Access
www.adpr-journal.com

radiation and re-emit it in the visible region. All-described Si QD properties could be exploited at the nanometric scale for the interaction with distinct matrixes (inorganic, organic, biological nature), taking advantage of their luminescent emission to provide an optical signal. In terms of the PL mechanisms, it has been shown that all three matrices can dominate the QCE. Generally, the main implications of confinement on the nanostructures are 1) broadening of wave factors, making the structure similar to a direct bandgap, that is, no need for phonon of intertransitions; and 2) It also results in the widening of the bandgap. This similarly causes an increase in the emission intensities due to the small size of QDs with well-defined energy levels. Each matrix also presents specific defects such as NBOHC, ODC, and E' centers in the oxide matrix, whereas band tails are in the case of the nitride matrix. For the carbide matrix, there is a decisive role of the composition ratio of Si/O/C in the matrix that could widely influence the emission properties of thin films. Moreover,

depending on the surrounding density and coalescence of QDs, the average size of particles is modified depending on the initial local environment. The shift in the luminescence spectra all over the visible region (blue, green, and red) shows a strong dependence on the resultant change in the size and/or the passivation environment of QDs. The passivation environment also plays an essential role in the final emission of these thin films. Depending on the environment around NPs, for instance, oxygen and hydrogen, the NPs' overall size could vary and modify consequently the bandgap and, hence, emission of these thin films. Generally, oxidation of the samples causes red emission, whereas hydrogen passivation results in green–yellow emission.

Si QDs are potent tools that can improve photoluminescent systems over traditional dye molecules or fluorescent proteins with more sensitive responses. The authors consider that a possible perspective on the improved use of Si QDs is to perform a deeper characterization of their interaction at the innermost part

Figure 17. a) Schematic view of FRET protease sensor based on Si QDs. Reproduced with permission.[205] Copyright 2017, SPIE. b) Selective imaging of pathogenic bacteria and the biofilms formation using Si QDs observed by optical and fluorescent technique. Reproduced under the terms of a Creative Commons Attribution CC-BY License.[206] Copyright 2022, The Authors, published by Frontiers.

**ADVANCED
SCIENCE NEWS**

www.advancedsciencenews.com

**ADVANCED
PHOTONICS
RESEARCH**
Open Access

www.adpr-journal.com

of cell tissues, where they could serve in applications to optimize cellular repair processes, cancer treatment evaluation, and diagnostics in real time, surpassing the possible cytotoxic effects that Si could trigger inside the host organism. A work published by Xiaou Cheng et al. reports the study of a protease sensor that combines nontoxic Si QDs with Förster resonance energy transfer (FRET).[205] The toxicity evaluated by cell viability assays (MTT) suggests a lack of acute toxicity for QDs' concentration up to 256 μg mL^{-1}, allowing the use of Si QDs as the donor and an organic dye as the acceptor modifying the emission (**Figure 17**a). Therefore, integrating Si materials properties and their emission mechanisms for application within the biological sectors can provide a solution for these research areas focused on biodetection. An example is the work of Jiayi Lin et al., who performed selective labeling of distinct bacteria and biofilms to distinguish between Gram-positive and Gram-negative bacteria (Figure 17b).[206]

Moreover, the convergence of many areas like nanomaterials engineering, microbiology, and biomedicine can provide innovations from a multidisciplinary perspective achieving proof-of-concept applications. Pathogen and virus detection has gained particular attention derived from the recent SARS-CoV2 pandemic and bacterial resistance, which are public concern issues that affect significantly the global population and must be promptly solved.[207] As discussed, Si-based compound nanomaterials offer advantages for fabricating biosensors and biomarkers (**Figure 18**). If simple labeling on bacteria or viruses can be observed through an optical response, this can contribute in a significant way to pathogen recognition as an efficient and easy-handle alternative to the existing methods (chromophores, labeled antibodies, fluorescent probes, among others), for use in places with limited resources.

At the same time, it is well known that Si is an element commonly found in traces; however, it is excreted from the organism
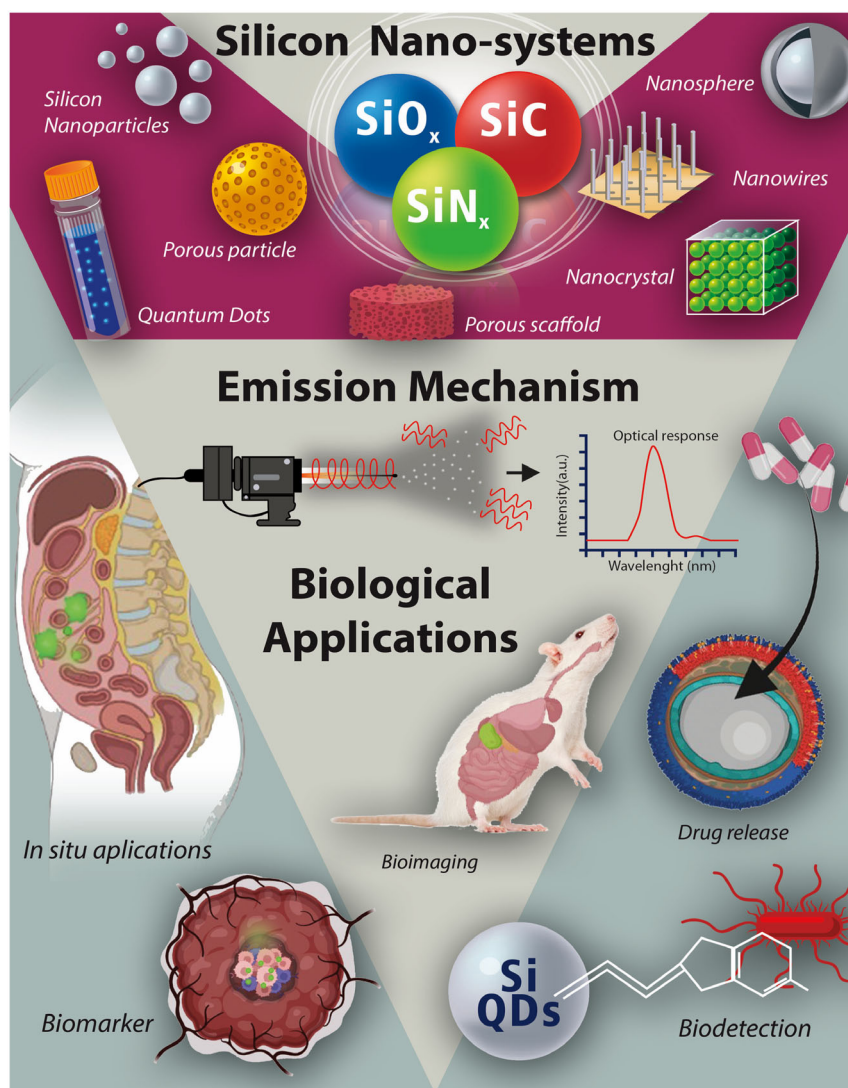
Figure 18. Graphical overview of the current and future perspectives in Si-based nanomaterials and their emission mechanisms to the extent of its application throughout the biological sector (Images taken from Biorender.com).

through urine. Considering those benefits, Si-based compound nanomaterials can be used for multiple in situ applications; nevertheless, an additional extensive study about cytotoxicity of these nanomaterials is required. The small size and matrix types (oxide, carbide, and nitride) could be decisive in applying these nanomaterials for specific biological applications. Once having a proper comprehension of the biocompatibility of these Si-based nanomaterials, the above-mentioned PL properties of QDs can be further explored for efficient and effective drug delivery systems.

Core–shell kind structures can also be designed to fabricate Si NPs and QDs drug-conjugated structures for the development of modern drugs. Likewise, using QDs with other materials can bring advantages since they could help overcome technical limitations in the described application sectors. Otherwise, though there are currently stacks of information about the use of QDs, the study of the optimization of this process and the generation of nanostructures for frequent use is still uncertain. Moreover, although many research groups are focused on QD improvement, there is a lack of information about the possible consequences of wastes generated from the QD synthesis processes, which could be used for new applications. Another challenge is the interaction of these nanostructures to understand cellular behavior from a single cell, which arises from the need to label proteins and tissues with highly stable dyes that can maintain their activity without compromising their functions.

In addition, it has been reported that NPs in the form of nanoneedles enhance the internalization of biomolecular markers through endocytosis to explore other aspects of intracellular interaction. Sahana Gopal et al. reported a study that aimed to extend the understanding of how nanoneedles modulate biological processes to mediate interaction with the intracellular space to develop cell manipulation technologies.[208] Moreover, Wei Sun et al. reported the directed use of differential interference contrast (DIC) microscopy to observe the entire endocytosis process of mesoporous Si NPs into living human lung cancer cells (A549) without fluorescence staining. It was observed that outside the cell, Si NPs follow a Brownian motion in the cell growth medium, but on the cell membrane, the movement is limited. This lowered mobility was due to the cytoplasm viscosity and the obstacles from the cellular cytoskeleton networks.[209] More studies about Si matrices and new configurations must be carried out to characterize in depth to improve the selectivity for targeted drug delivery based on endocytosis.

In addition to their excellent PL properties as nanomaterials, Si NPs have proved to be safe, as recognized by the US Food and Drug Administration (FDA), and highly tolerable for the human body. Since 2007, clinical trials in humans have demonstrated Si NPs' efficiency to be used as drug carriers,[210,211] as effectors for photothermal ablation of cancer tumors,[212–214] and as tracers of tumors for imaging and visualization during patients' biopsy.[215,216] The successful trials in humans have allowed that Si NPs-based formulations can be approved for phase I and phase II clinical trials.[217]

Conflict of Interest

The authors declare no conflict of interest.

[1] E. Mostafavi, P. Soltantabar, T. J. Webster, *Biomaterials in Translational Medicine*, Academic Press, USA **2019**, pp. 193–214.

[2] S. Sindhwani, W. C. W. Chan, *J. Intern. Med.* **2021**, *290*, 486.

[3] A. A. H. Abdellatif, H. M. Tawfeek, M. A. Younis, M. Alsharidah, O. Al Rugaie, *Int. J. Nanomed.* **2022**, *17*, 1951.

[4] S. Filali, F. Pirot, P. Miossec, *Trends Biotechnol.* **2020**, *38*, 163.

[5] S. Sarwat, F. J. Stapleton, M. D. P. Willcox, P. B. O'mara, R. D. Tilley, J. J. Gooding, M. Roy, *Nanomaterials* **2022**, *12*, 1965.

[6] M. B. Gongalsky, L. A. Osminkina, A. Pereira, A. A. Manankov, A. A. Fedorenko, A. N. Vasiliev, V. V. Solovyev, A. A. Kudryavtsev, M. Sentis, A. V. Kabashin, V. Y. Timoshenko, *Sci. Rep.* **2016**, *6*, 24732.

[7] S. Chinnathambi, S. Chen, S. Ganesan, N. Hanagata, *Adv. Healthcare Mater.* **2014**, *3*, 10.

[8] M. Fujii, R. Fujii, M. Takada, H. Sugimoto, *ACS Appl. Nano Mater.* **2020**, *3*, 6099.

[9] H. M. Gil, T. W. Price, K. Chelani, J.-S. G. Bouillard, S. D. J. Calaminus, G. J. Stasiuk, *iScience* **2021**, *24*, 102189.

[10] M. R. Younis, G. He, J. Lin, P. Huang, *Front. Chem.* **2020**, *8*, 424.

[11] I. T. Cheong, J. Mock, M. Kallergi, E. Groß, A. Meldrum, B. Rieger, M. Becherer, J. G. C. Veinot, *Adv. Opt. Mater.* **2023**, *11*, 2201834.

[12] H. Weman, B. Monemar, G. S. Oehrlein, S. J. Jeng, *Phys. Rev. B* **1990**, *42*, 3109.

[13] A. G. Cullis, L. T. Canham, *Nature* **1991**, *353*, 335.

[14] S. Takeoka, M. Fujii, S. Hayashi, *Phys. Rev. B* **2000**, *62*, 16820.

[15] S. M. Sze, K. K. Ng, *Physics of Semiconductor Devices*, 3rd ed., Wiley, USA **2006**.

[16] A. R. Barron, *Adv. Funct. Mater.* **1996**, *6*, 101.

[17] L. A. Leventhal, in *Simulation* **1976**, *27*, pp. 65–71.

[18] H. I. Hanafi, S. Tiwari, I. Khan, *IEEE Trans. Electron Devices* **1996**, *43*, 1553.

[19] L. T. Canham, *Appl. Phys. Lett.* **1990**, *57*, 1046.

[20] H. Takagi, H. Ogawa, Y. Yamazaki, A. Ishizaki, T. Nakagiri, *Appl. Phys. Lett.* **1990**, *56*, 2379.

[21] L. Pavesi, D. J. Lockwood, *Silicon Photonics*, Vol. 1, Springer-Verlag, Berlin **2004**.

[22] A. Dutt, Y. Matsumoto, S. Godavarthi, G. Santana-Rodríguez, J. Santoyo-Salazar, A. Escobosa, *Mater. Lett.* **2014**, *131*, 295.

[23] M. Pérez, A. Dutt, B. de Mora, E. Mon-Pérez, M. Villagrán-Muniz, M. F. García-Sánchez, G. Santana, *Mater. Lett.* **2018**, *216*, 277.

[24] E. Mon-Pérez, J. Salazar, E. Ramos, J. S. Salazar, A. L. Suárez, A. Dutt, G. Santana, B. M. Monroy, *Nanotechnology* **2016**, *27*, 455703.

[25] A. Ortiz-Santos, C. Ramos, J. Sastré-Hernández, G. Santana, A. Dutt, *Mater. Technol.* **2020**, *35*, 777.

[26] Y. Matsumoto, A. Dutt, G. Santana-Rodríguez, J. Santoyo-Salazar, M. Aceves-Mijares, *Appl. Phys. Lett.* **2015**, *106*, 171912.

[27] A. Dutt, Y. Matsumoto, E. Ramos, B. M. Monroy, J. S. Salazar, *Phys. Chem. Chem. Phys.* **2017**, *19*, 1526.

[28] J. R. Ramos-Serrano, Y. Matsumoto, A. Méndez-Blas, A. Dutt, C. Morales, A. I. Oliva, *J. Alloys Compd.* **2019**, *780*, 341.

[29] Y. Matsumoto, S. Asahi, T. Kita, J. Santoyo-Salazar, C. Ramos, B. Verma, J. R. Ramos-Serrano, S. Godavarthi, G. Santana, A. Dutt, *Physica E* **2019**, *111*, 179.

[30] A. E. Kaloyeros, Y. Pan, J. Goff, B. Arkles, *ECS J. Solid State Sci. Technol.* **2020**, *9*, 063006.

[31] H. Tamura, M. Rückschloss, T. Wirschem, S. Veprek, *Appl. Phys. Lett.* **1994**, *65*, 1537.

[32] J. L. Heinrich, C. L. Curtis, G. M. Credo, K. L. Kavanagh, M. J. Sailor, *Science* **1992**, *255*, 66.

[33] M. A. Tischler, R. T. Collins, J. H. Stathis, J. C. Tsang, *Appl. Phys. Lett.* **1992**, *60*, 639.

[34] T. Shimizu-Iwayama, M. Ohshima, T. Niimi, S. Nakao, K. Saitoh, T. Fujita, N. Itoh, *J. Phys.: Condens. Matter* **1993**, *5*, L375.

[35] M. L. Brongersma, A. Polman, K. S. Min, H. A. Atwater, *J. Appl. Phys.* **1999**, *86*, 759.

[36] S. Guha, S. B. Qadri, R. G. Musket, M. A. Wall, T. Shimizu-Iwayama, *J. Appl. Phys.* **2000**, *88*, 3954.

[37] R. Smirani, F. Martin, G. Abel, Y. Q. Wang, M. Chicoine, G. G. Ross, *J. Lumin.* **2005**, *115*, 62.

[38] Y. Yang, L. Xu, F. Yang, W. Liu, J. Xu, Z. Ma, K. Chen, *J. Non-Cryst. Solids* **2010**, *356*, 2790.

[39] L. Wang, Z. Ma, X. Huang, Z. Li, J. Li, Y. Bao, J. Xu, W. Li, K. Chen, *Solid State Commun.* **2001**, *117*, 239.

[40] Y. Matsumoto, S. Godavarthi, M. Ortega, V. Sánchez, S. Velumani, P. S. Mallick, *Thin Solid Films* **2011**, *519*, 4498.

[41] S. Kim, D. H. Shin, C. O. Kim, S. H. Hong, S.-H. Choi, *Thin Solid Films* **2012**, *520*, 3000.

[42] V. Nikas, S. Gallis, M. Huang, A. E. Kaloyeros, A. P. D. Nguyen, A. Stesmans, V. V. Afanas'ev, *Appl. Phys. Lett.* **2014**, *104*, 061906.

[43] A. Karakuscu, R. Guider, L. Pavesi, G. D. Sorarù, *J. Am. Ceram. Soc.* **2009**, *92*, 2969.

[44] Y. Ding, T. Kobayashi, H. Jia, H. Shirai, *ECS Trans.* **2009**, *23*, 1115.

[45] D. König, J. Rudd, M. A. Green, G. Conibeer, *Sol. Energy Mater. Sol. Cells* **2009**, *93*, 753.

[46] P. Pirasteh, J. Charrier, Y. Dumeige, J.-L. Doualan, P. Camy, O. Debieu, C. Liang, L. Khomenkova, J. Lemaitre, Y. G. Boucher, F. Gourbilleau, *J. Appl. Phys.* **2013**, *114*, 014906.

[47] J. A. Luna-López, G. García-Salgado, T. Díaz-Becerril, J. C. López, D. E. Vázquez-Valerdi, H. Juárez-Santiesteban, E. Rosendo-Andrés, A. Coyopol, *Mater. Sci. Eng., B* **2010**, *174*, 88.

[48] Y. Yu, R. Luo, H. Shang, *Appl. Surf. Sci.* **2016**, *368*, 325.

[49] C.-W. Jiang, M. A. Green, *J. Appl. Phys.* **2006**, *99*, 114902.

[50] F. Sohrabi, A. Nikniazi, H. Movl, *Solar Cells - Research and Application Perspectives*, In Tech, Rijeka, Croatia **2013**.

[51] G. Conibeer, M. Green, R. Corkish, Y. Cho, E. C. Cho, C. W. Jiang, T. Fangsuwannarak, E. Pink, Y. Huang, T. Puzzer, T. Trupke, B. Richards, A. Shalav, K. Lung Lin, *Thin Solid Films* **2006**, *511–512*, 654.

[52] E. Mon-Pérez, A. Dutt, J. Santoyo-Salazar, M. Sánchez, G. Santana, *Mater. Lett.* **2017**, *203*, 50.

[53] G. Franzò, A. Irrera, E. C. Moreira, M. Miritello, F. Iacona, D. Sanfilippo, G. Di Stefano, P. G. Fallica, F. Priolo, *Appl. Phys. A* **2002**, *74*, 1.

[54] E. Ojeda-Durán, K. Monfil-Leyva, J. Carrillo-López, A. Benítez-Lara, G. García-Salgado, J. A. Luna-López, *Silicon* **2019**, *11*, 2087.

[55] M. Dutta, in *Advances in Energy Materials* (Ed: J. S. Ikhmayies), Springer Nature, Cham, Switzerland **2020**, pp. 135–157.

[56] P. R. Huang, Y. C. Chen, K. Y. Kuo, P. T. Lee, *Sol. Energy Mater. Sol. Cells* **2019**, *193*, 287.

[57] X. Chen, P. Yang, *J. Mater. Sci.: Mater. Electron.* **2015**, *26*, 4604.

[58] N. Chiodini, F. Meinardi, F. Morazzoni, A. Paleari, R. Scotti, D. Di Martino, *Appl. Phys. Lett.* **2000**, *76*, 3209.

[59] V. Lehmann, U. Gösele, *Appl. Phys. Lett.* **1991**, *58*, 856.

[60] W. D. A. M. de Boer, D. Timmerman, K. Dohnalová, I. N. Yassievich, H. Zhang, W. J. Buma, T. Gregorkiewicz, *Nat. Nanotechnol.* **2010**, *5*, 878.

[61] A. Rodriguez-Gómez, A. García-Valenzuela, E. Haro-Poniatowski, J. C. Alonso-Huitrón, *J. Appl. Phys.* **2013**, *113*, 233102.

[62] D. Riabinina, C. Durand, J. Margot, M. Chaker, G. A. Botton, F. Rosei, *Phys. Rev. B* **2006**, *74*, 075334.

[63] A. G. Cullis, L. T. Canham, P. D. J. Calcott, *J. Appl. Phys.* **1997**, *82*, 909.

[64] G. Ledoux, O. Guillois, D. Porterat, C. Reynaud, F. Huisken, B. Kohn, V. Paillard, *Phys. Rev. B* **2000**, *62*, 15942.

[65] C. Delerue, G. Allan, M. Lannoo, *Phys. Rev. B* **1993**, *48*, 11024.

[66] F. Koch, V. Petrova-Koch, T. Muschik, *J. Lumin.* **1993**, *57*, 271.

[67] Y. Kanemitsu, T. Ogawa, K. Shiraishi, K. Takeda, *Phys. Rev. B* **1993**, *48*, 4883.

[68] G. Seguini, S. Schamm-Chardon, P. Pellegrino, M. Perego, *Appl. Phys. Lett.* **2011**, *99*, 082107.

[69] Y. R. Choi, M. Zheng, F. Bai, J. Liu, E. S. Tok, Z. Huang, C. H. Sow, *Sci. Rep.* **2014**, *4*, 4940.

[70] S. A. Cabanas-Tay, L. Palacios-Huerta, J. A. Luna-López, M. Aceves-Mijares, S. Alcántara-Iniesta, S. A. Pérez-García, A. Morales-Sánchez, *Semicond. Sci. Technol.* **2015**, *30*, 065009.

[71] K. Dohnalová, A. N. Poddubny, A. A. Prokofiev, W. D. De Boer, C. P. Umesh, J. M. Paulusse, H. Zuilhof, T. Gregorkiewicz, *Light Sci. Appl.* **2013**, *2*, e47.

[72] H. Imai, K. Arai, H. Imagawa, H. Hosono, Y. Abe, *Phys. Rev. B: Condens. Matter* **1988**, *38*, 12772.

[73] M. Stapelbroek, D. L. Griscom, E. J. Friebele, G. H. Sigel, *J. Non-Cryst. Solids* **1979**, *32*, 313.

[74] J. R. E. P. O'Reilly, *Phys. Rev. B* **1983**, *27*, 3786.

[75] Y. Y. S. Munekumi, T. Yamanaka, Y. Shimogaichi, K. Nagasawa, *J. Appl. Phys* **1990**, *68*, 1212.

[76] S. M. Prokes, W. E. Carlos, *J. Appl. Phys.* **1995**, *78*, 2671.

[77] D. J. Wolford, B. A. Scott, J. A. Reimer, J. A. Bradley, *Physica B+C* **1983**, *117–118*, 920.

[78] C. Tsai, K.-H. Li, J. Sarathy, S. Shih, J. C. Campbell, B. K. Hance, J. M. White, *Appl. Phys. Lett.* **1991**, *59*, 2814.

[79] M. V. Wolkin, J. Jorne, P. M. Fauchet, G. Allan, C. Delerue, *Phys. Rev. Lett.* **1999**, *82*, 197.

[80] G. Zatryb, A. Podhorodecki, X. J. Hao, J. Misiewicz, Y. S. Shen, M. A. Green, *Nanotechnology* **2011**, *22*, 335703.

[81] J. G. C. Veinot, *Chem. Commun.* **2006**, 4160.

[82] Y. Ma, X. Pi, D. Yang, *J. Phys. Chem. C* **2012**, *116*, 5401.

[83] D. König, J. Rudd, M. A. Green, G. Conibeer, *Phys. Rev. B* **2008**, *78*, 35339.

[84] Z. Ni, X. Pi, D. Yang, *RSC Adv.* **2012**, *2*, 11227.

[85] D. Jurbergs, E. Rogojina, L. Mangolini, U. Kortshagen, *Appl. Phys. Lett.* **2006**, *88*, 233116.

[86] A. R. Wilkinson, R. G. Elliman, in *Materials Research Society Symp. - Proc.*, vol. *770* **2003**, p. 81.

[87] J. A. Rodríguez, M. A. Vásquez-Agustín, A. Morales-Sánchez, M. Aceves-Mijares, *J. Nanomater.* **2014**, *2014*, 409482.

[88] M. Lannoo, C. Delerue, G. Allan, *J. Lumin.* **1996**, *70*, 170.

[89] R. Limpens, S. L. Luxembourg, A. W. Weeber, T. Gregorkiewicz, *Sci. Rep.* **2016**, *6*, 19566.

[90] R. Limpens, A. Lesage, M. Fujii, T. Gregorkiewicz, *Sci. Rep.* **2015**, *5*, 17289.

[91] Y. Nishi, *Jpn. J. Appl. Phys.* **1971**, *10*, 52.

[92] K. L. Brower, *Phys. Rev. B* **1988**, *38*, 9657.

[93] E. H. Poindexter, *Z. Phys. Chem.* **1987**, *151*, 165.

[94] A. Gupta, M. T. Swihart, H. Wiggers, *Adv. Funct. Mater.* **2009**, *19*, 696.

[95] R. Guerra, E. Degoli, S. Ossicini, *Phys. Rev. B* **2009**, *80*, 155332.

[96] R. Soulairol, F. Cleri, *Solid State Sci.* **2010**, *12*, 163.

[97] S. Cheylan, R. G. Elliman, *Nucl. Instrum. Methods Phys. Res., Sect. B* **2001**, *175–177*, 422.

[98] X. Wu, A. Bek, A. Bittner, C. Eggs, C. Ossadnik, S. Veprek, *Thin Solid Films* **2003**, *425*, 175.

[99] I. Pelant, *Phys. Status Solidi A* **2011**, *208*, 625.

[100] T. Torchynska, F. G. Becerril Espinoza, Y. Goldstein, E. Savir, J. Jedrzejewski, L. Khomenkova, N. Korsunska, V. Yukhimchuk, *Physica B* **2003**, *340–342*, 1119.

[101] F. Koch, V. Petrova-Koch, *J. Non-Cryst. Solids* **1996**, *198–200*, 840.

[102] A. Puzder, A. J. Williamson, J. C. Grossman, G. Galli, *Phys. Rev. Lett.* **2002**, *88*, 97401.

[103] B. Ghosh, N. Shirahata, *Crystals* **2020**, *10*, 143.

[104] L. Esaki, R. Tsu, *IBM J. Res. Dev.* **1970**, *14*, 61.

[105] R. Dingle, W. Wiegmann, C. H. Henry, *Phys. Rev. Lett.* **1974**, *33*, 827.

[106] M. H. Brodsky, *Solid State Commun.* **1980**, *36*, 55.

[107] X. X. Wang, J. G. Zhang, L. Ding, B. W. Cheng, W. K. Ge, J. Z. Yu, Q. M. Wang, *Phys. Rev. B* **2005**, *72*, 195313.

[108] X. Y. Chen, Y. F. Lu, L. J. Tang, Y. H. Wu, B. J. Cho, X. J. Xu, J. R. Dong, W. D. Song, *J. Appl. Phys.* **2005**, *97*, 014913.

[109] Z. X. Cao, R. Song, L. B. Ma, Y. Du, A. L. Ji, Y. Q. Wang, *Nanotechnology* **2006**, *17*, 2073.

[110] F. Iacona, C. Bongiorno, C. Spinella, S. Boninelli, F. Priolo, *J. Appl. Phys.* **2004**, *95*, 3723.

[111] M. Bedjaoui, B. Despax, M. Caumont, C. Bonafos, *Eur. Phys. J. Appl. Phys.* **2006**, *34*, 147.

[112] N.-M. Park, C.-J. Choi, T.-Y. Seong, S.-J. Park, *Phys. Rev. Lett.* **2001**, *86*, 1355.

[113] Y. Wang, D. Shen, Y. Liu, J. Zhang, Z. Zhang, Y. Liu, Y. Lu, X. Fan, *Physica E* **2005**, *27*, 284.

[114] C. Liu, C. Li, A. Ji, L. Ma, Y. Wang, Z. Cao, *Nanotechnology* **2005**, *16*, 940.

[115] G. Santana, B. M. Monroy, A. Ortiz, L. Huerta, J. C. Alonso, J. Fandiño, J. Aguilar-Hern´ndez, E. Hoyos, F. Cruz-Gandarilla, G. Contreras-Puentes, *Appl. Phys. Lett.* **2006**, *88*, 041916.

[116] B. M. Monroy, G. Santana, A. Benami, A. Ortiz, J. C. Alonso, J. Fandiño, F. Cruz-Gandarilla, J. Aguilar-Hernández, G. Contreras-Puente, A. López-Suárez, A. Oliver, *J. Nanosci. Nanotechnol.* **2009**, *9*, 2902.

[117] A. Benami, G. Santana, B. M. Monroy, A. Ortiz, J. C. Alonso, J. Fandiño, J. Aguilar-Hernández, G. Contreras-Puente, *Physica E* **2007**, *38*, 148.

[118] L. V. Goncharova, P. H. Nguyen, V. L. Karner, R. D'Ortenzio, S. Chaudhary, C. R. Mokry, P. J. Simpson, *J. Appl. Phys.* **2015**, *118*, 224302.

[119] A. Muñoz-Rosas, A. Rodríguez-Gómez, J. Alonso-Huitrón, *Nanomaterials* **2018**, *8*, 182.

[120] A. V. Vasin, A. V. Rusavsky, D. V. Kysil, S. Prucnal, Y. P. Piryatinsky, S. P. Starik, I. Nasieka, V. V. Strelchuk, V. S. Lysenko, A. N. Nazarov, *J. Lumin.* **2017**, *191*, 102.

[121] M. Jain, J. R. Ramos-Serrano, A. Dutt, Y. Matsumoto, in *2020 17th Inter. Conf. on Electrical Engineering, Computing Science and Automatic Control (CCE)*, Mexico City, Mexico, November **2020**, pp. 1–6.

[122] V. Nikas, S. Gallis, M. Huang, A. E. Kaloyeros, A. P. D. Nguyen, A. Stesmans, V. V. Afanas'ev, *Appl. Phys. Lett.* **2014**, *104*, 061906.

[123] A. Coyopol, G. Garcia-Salgado, T. Díaz-Becerril, M. A. Vásquez-Agustín, R. Romano-Trujillo, R. López, E. Rosendo, F. G. Nieto-

[124] K. C. Liu, H. L. Cheng, J. R. Tsai, Y. L. Chiang, Y. C. Hsieh, D. J. Jan, *Thin Solid Films* **2010**, *518*, 6195.

[125] Y. Iwase, T. Fuchigami, Y. Horie, Y. Daiko, S. Honda, Y. Iwamoto, *Materials* **2019**, *12*, 1721.

[126] S. H. Mir, L. A. Nagahara, T. Thundat, P. Mokarian-Tabari, H. Furukawa, A. Khosla, *J. Electrochem. Soc.* **2018**, *165*, B3137.

[127] U. Díaz, A. Corma, *Chem. Eur. J.* **2018**, *24*, 3944.

[128] J. Zhou, X. Zheng, Z. Shi, B. Zhao, F. Liu, Y. Li, *Int. J. Mod. Phys. B* **2011**, *25*, 2149.

[129] S. L. Shevchuk, Y. P. Maishev, *Thin Solid Films* **2005**, *492*, 114.

[130] G.-R. Lin, Y.-H. Pai, C.-T. Lin, C.-C. Chen, *Appl. Phys. Lett.* **2010**, *96*, 263514.

[131] B. H. Kim, C. H. Cho, T. W. Kim, N. M. Park, G. Y. Sung, S. J. Park, *Appl. Phys. Lett.* **2005**, *86*, 091908.

[132] M. Jain, J. R. Ramos-serrano, A. Dutt, Y. Matsumoto, *Mater. Lett.* **2021**, *291*, 129547.

[133] M. Arango-ospina, F. Xie, I. Gonzalo-juan, R. Riedel, E. Ionescu, A. R. Boccaccini, *Appl. Mater. Today* **2020**, *18*, 100482.

[134] A. Tamayo, R. Ruiz-Caro, A. Mazo, M. D. Veiga-Ochoa, J. Rubio, *J. Mater. Sci.* **2016**, *51*, 1382.

[135] R. Riedel, L. Toma, E. Janssen, J. Nuffer, T. Melz, H. Hanselka, *J. Am. Ceram. Soc.* **2010**, *93*, 920.

[136] P. Lagonegro, F. Rossi, C. Galli, A. Smerieri, R. Alinovi, S. Pinelli, T. Rimoldi, G. Attolini, *Mater. Sci. Eng., C* **2017**, *73*, 465.

[137] M. Nastasi, Q. Su, L. Price, J. A. Colón, T. Chen, R. Balerio, L. Shao, *J. Nucl. Mater.* **2015**, *461*, 200.

[138] M. Nakaya, K. Kodama, S. Yasuhara, A. Hotta, *J. Polym.* **2016**, *2016*, 1.

[139] M. Nakaya, S. Yasuhara, T. Maeda, A. Hotta, *Surf. Coat. Technol.* **2018**, *344*, 21.

[140] V. S. Pradeep, M. Graczyk-zajac, R. Riedel, G. D. Sorarù, *Electrochim. Acta* **2014**, *119*, 78.

[141] C. Chandra, J. Kim, *Chem. Eng. J.* **2018**, *338*, 126.

[142] J. Huang, K. Leng, Y. Chen, L. Chen, S. Liu, S. Khan, D. Wu, R. Fu, *J. Mater. Chem. A* **2019**, *7*, 22950.

[143] F. Roth, C. Schmerbauch, E. Ionescu, N. Nicoloso, O. Guillon, R. Riedel, *J. Sens. Sens. Syst.* **2015**, *4*, 133.

[144] H. Miyazaki, *Jpn. J. Appl. Phys.* **2008**, *47*, 8287.

[145] F. A. Memon, F. Morichetti, A. Melloni, *ACS Photonics* **2018**, *5*, 2755.

[146] L. Baudzus, P. M. Krummrich, *Opt. Mater. Express* **2019**, *9*, 2797.

[147] S. Hayashi, M. Kataoka, K. Yamamoto, *Jpn. J. Appl. Phys.* **1993**, *32*, L274.

[148] S. Hayashi, M. Kataoka, H. Koshida, K. Yamamoto, *Surf. Rev. Lett.* **1996**, *3*, 1095.

[149] B. Garrido, M. López., S. Ferré, A. Romano-Rodríguez, A. Pérez-Rodríguez, P. Ruterana, J. R. Morante, *Nucl. Instrum. Methods Phys. Res., Sect. B* **1996**, *120*, 101.

[150] M. López, B. Garrido, C. Bonafos, O. González-Varona, A. Pérez-Rodríguez, R. Rodríguez, P. Ruterana, J. R. Morante, *MRS Online Proc. Lib.* **1998**, *486*, 237.

[151] A. P. Rodrguez, O. González-Varona, B. Garrido, P. Pellegrino, J. R. Morante, C. Bonafos, M. Carrada, A. Claverie, *J. Appl. Phys.* **2003**, *94*, 254.

[152] J. Zhao, D. S. Mao, Z. X. Lin, B. Y. Jiang, Y. H. Yu, X. H. Liu, H. Z. Wang, G. Q. Yang, *Appl. Phys. Lett.* **1998**, *73*, 1838.

[153] L. Rebohle, T. Gebel, H. Fröb, H. Reuther, W. Skorupa, *Appl. Surf. Sci.* **2001**, *184*, 156.

[154] S. Wang, C. Zhang, Z. Wang, X. Zu, *Optoelectron. Adv. Mater. Rapid Commun.* **2010**, *4*, 771.

[155] A. J. Kontkiewicz, A. M. Kontkiewicz, J. Siejka, S. Sen, G. Nowak, A. M. Hoff, P. Sakthivel, K. Ahmed, P. Mukherjee, S. Witanachchi, J. Lagowski, *Appl. Phys. Lett.* **1994**, *65*, 1436.

[156] Y. P. Guo, J. C. Zheng, A. T. S. Wee, C. H. A. Huan, K. Li, J. S. Pan, Z. C. Feng, S. J. Chua, *Chem. Phys. Lett.* **2001**, *339*, 319.

[157] S. Gallis, V. Nikas, H. Suhag, M. Huang, A. E. Kaloyeros, *Appl. Phys. Lett.* **2010**, *97*, 081905.

[158] Z. Lin, Y. Guo, J. Song, Y. Zhang, C. Song, X. Wang, R. Huang, *J. Non-Cryst. Solids* **2015**, *428*, 184.

[159] Z. Lin, Y. Guo, C. Song, J. Song, X. Wang, Y. Zhang, R. Huang, X. Huang, *J. Alloys Compd.* **2015**, *633*, 153.

[160] Z. Lin, R. Huang, H. Wang, Y. Wang, Y. Zhang, Y. Guo, J. Song, C. Song, H. Li, *J. Alloys Compd.* **2017**, *694*, 946.

[161] L. Palacios-Huerta, S. A. Cabañas-Tay, M. A. Cardona-Castro, M. Aceves-Mijares, C. Domínguez-Horna, A. Morales-Sánchez, *Appl. Phys. Lett.* **2016**, *109*, 031906.

[162] A. Podhorodecki, J. Misiewicz, F. Gourbilleau, R. Rizk, *Electrochem. Solid-State Lett.* **2008**, *11*, 60.

[163] J. D. Holmes, K. J. Ziegler, R. C. Doty, L. E. Pell, K. P. Johnston, B. A. Korgel, *J. Am. Chem. Soc.* **2001**, *123*, 3743.

[164] X. Liu, J. Zhang, Z. Yan, S. Ma, Y. Wang, *Mater. Phys. Mech.* **2001**, *4*, 85.

[165] S. Y. Seo, K. S. Cho, J. H. Shin, *Appl. Phys. Lett.* **2004**, *84*, 717.

[166] S. Gallis, V. Nikas, A. Kaloyeros, in *Modern Technologies for Creating the Thin-film Systems and Coatings* (Ed: N. N. Nikitenkov), IntechOpen, London, UK **2017**, pp. 277–302.

[167] P. G. Pai, S. S. Chao, Y. Takagi, G. Lucovsky, *J. Vac. Sci. Technol., A* **1986**, *4*, 689.

[168] W. Kaiser, P. H. Keck, C. F. Lange, *Phys. Rev.* **1956**, *101*, 1264.

[169] A. P. Baraban, S. N. Samarin, V. A. Prokofiev, V. A. Dmitriev, A. A. Selivanov, Y. Petrov, *J. Lumin.* **2019**, *205*, 102.

[170] Z. Liu, C. Davis, W. Cai, L. He, X. Chen, H. Dai, *Proc. Natl. Acad. Sci. USA* **2008**, *105*, 1410.

[171] H. Ma, X. Li, X. Liu, M. Deng, X. Wang, A. Iqbal, W. Liu, W. Qin, *Sens. Actuators, B* **2018**, *255*, 1687.

[172] A. Shiohara, S. Hanada, S. Prabakar, K. Fujioka, T. H. Lim, K. Yamamoto, P. T. Northcote, R. D. Tilley, *J. Am. Chem. Soc.* **2010**, *132*, 248.

[173] F. Erogbogbo, K. Yong, I. Roy, R. Hu, W. Law, W. Zhao, H. Ding, F. Wu, R. Kumar, M. T. Swihart, P. N. Prasad, *ACS Nano* **2011**, *5*, 413.

[174] Y. K. Dou, Y. Chen, X. W. He, W. Y. Li, Y. H. Li, Y. K. Zhang, *Anal. Chem.* **2017**, *89*, 11286.

[175] V. Skryshevsky, T. Serdiuk, Y. Zakharko, S. Alekseev, A. Géloën, V. Lysenko, in *Functional Nanomaterials and Devices for Electronics, Sensors and Energy Harvesting*, Springer, Cham, Switzerland **2014**, pp. 323–348.

[176] Q. He, Z. Zhang, F. Gao, Y. Li, J. Shi, *Small* **2011**, *7*, 271.

[177] A. M. Derfus, W. C. W. Chan, S. N. Bhatia, *Nano Lett.* **2004**, *4*, 11.

[178] A. S. Ballou, B. Lagerholm, B. C. Ernst, L. A. Bruchez, M. P. Waggoner, *Bioconjugate Chem.* **2004**, *15*, 79.

[179] C. A. Poland, R. Duffin, I. Kinloch, A. Maynard, W. A. H. Wallace, A. Seaton, V. Stone, S. Brown, W. MacNee, K. Donaldson, *Nat. Nanotechnol.* **2008**, *3*, 423.

[180] H. Liang, C. Jin, Y. Tang, F. Wang, C. Ma, Y. Yang, *J. Appl. Toxicol.* **2014**, *34*, 367.

[181] H. Soo Choi, W. Liu, P. Misra, E. Tanaka, J. P. Zimmer, B. Itty Ipe, M. G. Bawendi, J. V. Frangioni, *Nat. Biotechnol.* **2007**, *25*, 1165.

[182] J. Bouclé, A. Kassiba, J. Emery, I. V. Kityk, M. Makowska-Janusik, J. Sanetra, N. Herlin-Boime, M. Mayne, *Phys. Lett. A* **2002**, *302*, 196.

[183] T. K. Nguyen, H. P. Phan, H. Kamble, R. Vadivelu, T. Dinh, A. Iacopi, G. Walker, L. Hold, N. T. Nguyen, D. V. Dao, *ACS Appl. Mater. Interfaces* **2017**, *9*, 41641.

[184] H. Uğuz, A. Goyal, T. Meenpal, I. W. Selesnick, R. G. Baraniuk, N. G. Kingsbury, A. Haiter Lenin, S. Mary Vasanthi, T. Jayasree, M. Adam, E. Y. K. Ng, S. L. Oh, M. L. Heng, Y. Hagiwara, J. H. Tan, J. W. K. Tong, U. R. Acharya, G. Cappiello, S. Das, E. B. Mazomenos, K. Maharatna, G. Koulaouzidis, J. Morgan, P. E. Puddu, M. A. Goda, P. Hajas, G. D. Clifford, C. Liu, B. Moody, D. Springer, et al., *J. Neural Eng.* **2017**, *14*, 056006.

[185] V. Nair, J. Yi, D. Isheim, M. Rotenberg, L. Meng, F. Shi, X. Chen, X. Gao, A. Prominski, Y. Jiang, J. Yue, C. T. Gallagher, D. N. Seidman, B. Tian, *Sci. Adv.* **2020**, *6*, https://doi.org/10.1126/sciadv.aaz2743.

[186] B. Ghezzi, P. Lagonegro, G. Attolini, P. M. Rotonda, C. Cornelissen, J. S. Ponraj, L. Parisi, G. Passeri, F. Rossi, G. M. Macaluso, *Mater. Sci. Eng., C* **2021**, *121*, 111772.

[187] P. Zrazhevskiy, X. Gao, *Nat. Commun.* **2013**, *4*, 1619.

[188] T. Serdiuk, V. Lysenko, B. Mognetti, V. Skryshevsky, A. Géloën, *J. Biophotonics* **2013**, *6*, 291.

[189] J. Yoo, S. Han, W. Park, T. Lee, Y. Park, H. Chang, S. K. Hahn, W. Kwon, *ACS Appl. Mater. Interfaces* **2018**, *10*, 44247.

[190] E. J. Anglin, L. Cheng, W. R. Freeman, M. J. Sailor, *Adv. Drug Delivery Rev.* **2008**, *60*, 1266.

[191] C. Charnay, S. Bégu, C. Tourné-Péteilh, L. Nicole, D. A. Lerner, J. M. Devoisselle, *Eur. J. Pharm. Biopharm.* **2004**, *57*, 533.

[192] J. L. Coffer, J. L. Montchamp, J. B. Aimone, R. P. Weis, *Phys. Status Solidi A* **2003**, *197*, 336.

[193] L. Vaccari, D. Canton, N. Zaffaroni, R. Villa, M. Tormen, E. di Fabrizio, *Microelectron. Eng.* **2006**, *83*, 1598.

[194] P. Kowalik, I. Kamińska, K. Fronc, A. Borodziuk, M. Duda, T. Wojciechowski, K. Sobczak, D. Kalinowska, M. T. Klepka, B. Sikora, *Nanotechnology* **2021**, *32*, 475101.

[195] G. Pezzotti, B. J. McEntire, R. Bock, W. Zhu, F. Boschetto, A. Rondinella, E. Marin, Y. Marunaka, T. Adachi, T. Yamamoto, N. Kanamura, B. S. Bal, *ACS Biomater. Sci. Eng.* **2016**, *2*, 1121.

[196] Y. He, Y. Su, X. Yang, Z. Kang, T. Xu, R. Zhang, C. Fan, S. T. Lee, *J. Am. Chem. Soc.* **2009**, *131*, 4434.

[197] J. Liang, C. Huang, X. Gong, *ACS Sustainable Chem. Eng.* **2019**, *7*, 18213.

[198] Q. Li, T. Y. Luo, M. Zhou, H. Abroshan, J. Huang, H. J. Kim, N. L. Rosi, Z. Shao, R. Jin, *ACS Nano* **2016**, *10*, 8385.

[199] J. Herrera-Celis, C. Reyes-Betanzo, A. Torres-Jacome, A. Hernández-Flores, A. Itzmoyotl-Toxqui, V. Aca-Aca, O. Gelvez-Lizarazo, A. Culebro-Gomez, A. Zazueta-Gambino, A. Orduña-Díaz, J. Morales-Chávez, R. Salinas-Domínguez, S. Saddow, K. Noble, *J. Electrochem. Soc.* **2017**, *164*, B641.

[200] K. Chitra, G. Annadurai, *J. Nanotechnol.* **2013**, *2013*, 509628.

[201] V. Duplan, E. Frost, J. J. Dubowski, *Sens. Actuators, B* **2011**, *160*, 46.

[202] G. Pezzotti, R. M. Bock, B. J. McEntire, E. Jones, M. Boffelli, W. Zhu, G. Baggio, F. Boschetto, L. Puppulin, T. Adachi, T. Yamamoto, N. Kanamura, Y. Marunaka, B. S. Bal, *Langmuir* **2016**, *32*, 3024.

[203] G. Pezzotti, T. Asai, T. Adachi, E. Ohgitani, T. Yamamoto, N. Kanamura, F. Boschetto, W. Zhu, M. Zanocco, E. Marin, B. S. Bal, B. J. McEntire, K. Makimura, O. Mazda, I. Nishimura, *Acta Biomater.* **2021**, *126*, 259.

[204] T. Bělinová, I. Machová, D. Beke, A. Fučíková, A. Gali, Z. Humlová, J. Valenta, M. H. Kalbáčová, *Nanomaterials* **2020**, *10*, 573.

[205] X. Cheng, B. F. P. McVey, A. B. Robinson, G. Longatte, P. B. O'Mara, V. T. G. Tan, P. Thordarson, R. D. Tilley, K. Gaus, J. Justin Gooding, *J. Biomed. Opt.* **2017**, *22*, 087002.

[206] J. Lin, L. Xu, Y. Zheng, D. Wu, J. Yue, *Front. Bioeng. Biotechnol.* **2022**, *10*, https://doi.org/10.3389/fbioe.2022.971682.

[207] C. Gutiérrez Rodelo, R. A. Salinas, E. Armenta Jaime, S. Armenta, A. Galdámez-Martínez, S. E. Castillo-Blum, H. Astudillo-de la Vega, A. Nirmala Grace, C. A. Aguilar-Salinas, J. Gutiérrez Rodelo, G. Christie, W. F. Alsanie, G. Santana, V. K. Thakur, A. Dutt, *Coord. Chem. Rev.* **2022**, *457*, 214402.

**ADVANCED
SCIENCE NEWS**

www.advancedsciencenews.com

**ADVANCED
PHOTONICS
RESEARCH**
Open Access

www.adpr-journal.com

[208] S. Gopal, C. Chiappini, J. Penders, V. Leonardo, H. Seong, S. Rothery, Y. Korchev, A. Shevchuk, M. M. Stevens, *Adv. Mater.* **2019**, *31*, 1806788.

[209] W. Sun, N. Fang, B. G. Trewyn, M. Tsunoda, I. I. Slowing, V. S. Y. Lin, E. S. Yeung, *Anal. Bioanal. Chem.* **2008**, *391*, 2119.

[210] A. Tan, N. G. Eskandar, S. Rao, C. A. Prestidge, *Drug Delivery. Transl. Res.* **2014**, *4*, 212.

[211] K. Bukara, L. Schueller, J. Rosier, M. A. Martens, T. Daems, L. Verheyden, S. Eelen, M. Van Speybroeck, C. Libanati, J. A. Martens, G. Van Den Mooter, F. Frérart, K. Jolling, M. De Gieter, B. Bugarski, F. Kiekens, *Eur. J. Pharm. Biopharm.* **2016**, *108*, 220.

[212] A. N. Kharlamov, A. E. Tyurnina, V. S. Veselova, O. P. Kovtun, V. Y. Shur, J. L. Gabinsky, *Nanoscale* **2015**, *7*, 8003.

[213] A. N. Kharlamov, J. A. Feinstein, J. A. Cramer, J. A. Boothroyd, E. V. Shishkina, V. Shur, *Future Cardiol.* **2017**, *13*, 345.

[214] A. R. Rastinehad, H. Anastos, E. Wajswol, J. S. Winoker, J. P. Sfakianos, S. K. Doppalapudi, M. R. Carrick, C. J. Knauer, B. Taouli, S. C. Lewis, A. K. Tewari, J. A. Schwartz, S. E. Canfield, A. K. George, J. L. West, N. J. Halas, *Proc. Natl. Acad. Sci. USA* **2019**, *116*, 18590.

[215] D. K. Zanoni, H. E. Stambuk, B. Madajewski, P. H. Montero, D. Matsuura, K. J. Busam, K. Ma, M. Z. Turker, S. Sequeira, M. Gonen, P. Zanzonico, U. Wiesner, M. S. Bradbury, S. G. Patel, *JAMA Netw. Open* **2021**, *4*, e211936.

[216] E. Phillips, O. Penate-Medina, P. B. Zanzonico, R. D. Carvajal, P. Mohan, Y. Ye, J. Humm, M. Gönen, H. Kalaigian, H. Schöder, H. W. Strauss, S. M. Larson, U. Wiesner, M. S. Bradbury, *Sci. Transl. Med.* **2014**, *6*, 260ra149.

[217] T. I. Janjua, Y. Cao, C. Yu, A. Popat, *Nat. Rev. Mater.* **2021**, *6*, 1072.

[218] J. A. Jaramillo Gomez, T. V. Torchynska, J. L. Casas Espinola, J. A. Bentosa Gutiérrez, L. Khomenkova, A. Slaoui, *IOP Conf. Ser.: Mater. Sci. Eng.* **2017**, *169*, 012021.

[219] I. Parkhomenko, L. Vlasukova, F. Komarov, O. Milchanin, M. Makhavikou, A. Mudryi, V. Zhivulko, J. Żuk, P. Kopyciński, D. Murzalinov, *Thin Solid Films* **2017**, *626*, 70.

[220] J. Han, Y. J. Yin, D. Han, L. Z. Dong, *Mater. Res. Express* **2017**, *4*, 096301.

[221] M. Koutsoureli, S. Xavier, L. Michalas, C. Lioutas, S. Bansropun, G. Papaioannou, A. Ziaei, *J. Micromech. Microeng.* **2017**, *27*, 014001.

[222] H. Xia, D. Xiang, P. Mou, W. Yang, *Thin Solid Films* **2017**, *638*, 1.

[223] S. Van Nguyen, S. Hosadugra, T. Haigh, Y. Yao, L. Tai, S. Cohen, T. Shaw, C. K. Hu, E. Liniger, K. Virwani, A. J. Kellock, D. Canaperi, *ECS J. Solid State Sci. Technol.* **2017**, *6*, P429.

[224] C. Yang, J. Pham, *Silicon* **2018**, *10*, 2561.

[225] A. F. Braña, H. Gupta, R. K. Bommali, P. Srivastava, S. Ghosh, R. P. Casero, *Thin Solid Films* **2018**, *662*, 21.

[226] P. Wang, S. Jin, T. Lu, C. Cui, D. Yang, X. Yu, *J. Phys. D: Appl. Phys.* **2019**, *52*, 345102.

[227] B. Cossou, S. Jacques, G. Couégnat, S. W. King, L. Li, W. A. Lanford, G. Bhattarai, M. Paquette, G. Chollon, *Thin Solid Films* **2019**, *681*, 47.

[228] L. Vlasukova, I. Parkhomenko, F. Komarov, A. Akilbekov, D. Murzalinov, A. Mudryi, Y. Ryabikin, I. Romanov, S. Giniyatova, A. Dauletbekova, *Mater. Res. Express* **2018**, *5*, 096414.

[229] R. A. Ovanesyan, D. M. Hausmann, S. Agarwal, *J. Vac. Sci. Technol., A* **2017**, *35*, 021506.

[230] X. Meng, H. S. Kim, A. T. Lucero, S. M. Hwang, J. S. Lee, Y. C. Byun, J. Kim, B. K. Hwang, X. Zhou, J. Young, M. Telgenhoff, *ACS Appl. Mater. Interfaces* **2018**, *10*, 14116.

[231] T. Nagatsuka, H. Uzawa, D. Tanaka, Y. Oba, Y. Nishida, T. Iwasa, K. Ichi Tayama, T. Yoshida, T. Ezaki, Y. Seto, *Sens. Actuators, B* **2017**, *246*, 937.

[232] B. Yin, W. Xie, L. Liang, Y. Deng, S. He, F. He, D. Zhou, C. Tlili, D. Wang, *ACS Omega* **2017**, *2*, 7127.

[233] P. M. Dietrich, N. Lange, A. Lippitz, M. Holzweber, N. Kulak, W. E. S. Unger, *Appl. Surf. Sci.* **2019**, *481*, 10.

[234] H. I. Lee, J. B. Park, W. Xianyu, K. Kim, J. G. Chung, Y. K. Kyoung, S. Byun, W. Y. Yang, Y. Y. Park, S. M. Kim, E. Cho, J. K. Shin, *Sci. Rep.* **2017**, *7*, 14146.

[235] X. Li, D. Johnson, W. Ma, H. Chung, J. Getpreecharsawas, J. L. McGrath, A. A. Shestopalov, *Chem. Mater.* **2017**, *29*, 2294.

[236] H. Hoi, S. S. Rezaie, L. Gong, P. Sen, H. Zeng, C. Montemagno, M. Gupta, *Biosens. Bioelectron.* **2018**, *102*, 497.

[237] E.-C. Cho, M. A. Green, G. Conibeer, D. Song, Y. Cho, G. Scardera, S. Huang, S. Park, X. J. Hao, Y. Huang, L. Van Dao, *Adv. OptoElectron.* **2007**, *2007*, 069578.

[238] K. S. Min, K. V. Shcheglov, C. M. Yang, H. A. Atwater, M. L. Brongersma, A. Polman, *Appl. Phys. Lett.* **1996**, *69*, 2033.

[239] T.-W. Kim, C.-H. Cho, B.-H. Kim, S.-J. Park, *Appl. Phys. Lett.* **2006**, *88*, 123102.

[240] A. Mathur, D. Pal, A. Singh, R. Singh, S. Zollner, S. Chattopadhyay, *J. Vac. Sci. Technol., B* **2019**, *37*, 041802.

[241] I. Vivaldo, M. Moreno, A. Torres, R. Ambrosio, P. Rosales, N. Carlos, W. Calleja, K. Monfil, A. Benítez, *J. Lumin.* **2017**, *190*, 215.

[242] J. Alarcón-Salazar, R. López-Estopier, E. Quiroga-González, A. Morales-Sánchez, J. Pedraza-Chávez, I. E. Zaldívar-Huerta, M. Aceves-Mijares, in *Chemical Vapor Deposition - Recent Advances and Applications in Optical, Solar Cells and Solid State Devices*, IntechOpen, London, UK **2016**, p. 159.

[243] A. Dutt, Y. Matsumoto, J. Santoyo-Salazar, G. Santana-Rodríguez, S. Godavarthi, *Thin Solid Films* **2015**, *595*, 221.

[244] K.-C. Lin, S.-C. Lee, *J. Appl. Phys.* **1992**, *72*, 5474.

[245] C. Mo, L. Zhang, C. Xie, T. Wang, *J. Appl. Phys.* **1993**, *73*, 5185.

[246] S. V. Deshpande, E. Gulari, S. W. Brown, S. C. Rand, *J. Appl. Phys.* **1995**, *77*, 6534.

[247] Q. Liu, X. Chen, H. Li, Y. Guo, J. Song, W. Zhang, C. Song, R. Huang, Z. Lin, *Micromachines* **2021**, *12*, 354.

[248] A. V. Amosov, Y. N. Kulchin, A. V. Dvurechenskii, V. P. Dzyuba, *J. Lumin.* **2022**, *243*, 118615.

[249] D. V. Shuleiko, S. V. Zabotnov, D. M. Zhigunov, A. A. Zelenina, I. A. Kamenskih, P. K. Kashkarov, *Semiconductors* **2017**, *51*, 196.

[250] H. Gupta, O. Plantevin, R. K. Bommali, S. Ghosh, P. Srivastava, *Phys. Status Solidi B* **2020**, *257*, 1900378.

[251] C. H. Lin, W. Y. Uen, S. M. Lan, Y. C. Huang, S. M. Liao, Z. Y. Li, T. N. Yang, C. Te Ku, M. C. Chen, Y. H. Huang, *J. Appl. Phys.* **2009**, *105*, 053107.

[252] J. Kistner, X. Chen, Y. Weng, H. P. Strunk, M. B. Schubert, J. H. Werner, *J. Appl. Phys.* **2011**, *110*, 023520.

[253] L. V. Mercaldo, E. M. Esposito, P. D. Veneri, B. Rezgui, A. Sibai, G. Bremond, *J. Appl. Phys.* **2011**, *109*, 093512.

[254] X. Zeng, W. Liao, G. Wen, X. Wen, W. Zheng, *J. Appl. Phys.* **2014**, *115*, 154314.

[255] N. Hafsi, H. Bouridah, M. R. Beghoul, H. Haoues, *J. Appl. Phys.* **2015**, *117*, 063105.

[256] A. Rodriguez-Gómez, A. García-Valenzuela, E. Haro-Poniatowski, J. C. Alonso-Huitrón, *J. Appl. Phys.* **2013**, *113*, 233102.

[257] E. Mon-Pérez, J. Salazar, A. Dutt, J. Santoyo-Salazar, G. Santana, in *2017 IEEE 44th Photovoltaic Specialist Conf. (PVSC 2017)*, IEEE **2017**, pp. 370–372.

[258] R. Kumar Bommali, S. Preet Singh, S. Rai, P. Mishra, B. R. Sekhar, G. Vijaya Prakash, P. Srivastava, *J. Appl. Phys.* **2012**, *112*, 123518.

[259] A. Zelenina, S. A. Dyakov, D. Hiller, S. Gutsch, V. Trouillet, M. Bruns, S. Mirabella, P. Löper, L. López-Conesa, J. López-Vidrier, S. Estradé,

F. Peiró, B. Garrido, J. Bläsing, A. Krost, D. M. Zhigunov, M. Zacharias, *J. Appl. Phys.* **2013**, *114*, 184311.

[260] M. Sendova-Vassileva, N. Tzenov, D. Dimova-Malinovska, T. Marinova, V. Krastev, *Thin Solid Films* **1996**, *276*, 318.

[261] Y. H. Yu, S. P. Wong, I. H. Wilson, *Phys. Status Solidi A* **1998**, *168*, 531.

[262] S. Muto, A. V. Vasin, Y. Ishikawa, N. Shibata, J. Salonen, V. P. Lehto, *Mater. Sci. Forum* **2007**, *561–565*, 1127.

[263] A. V. Vasin, Y. Ishikawa, N. Shibata, J. Salonen, V. P. Lehto, *Jpn. J. Appl. Phys.* **2007**, *46*, 464.

[264] Y. Ishikawa, A. V. Vasin, J. Salonen, S. Muto, V. S. Lysenko, A. N. Nazarov, N. Shibata, V.-P. Lehto, *J. Appl. Phys.* **2008**, *104*, 083522.

[265] A. V. Vasin, V. I. Kushnirenko, V. S. Lysenko, A. N. Nazarov, Y. Ishikawa, J. Salonen, *Tech. Phys. Lett.* **2009**, *35*, 559.

[266] A. V. Vasin, P. N. Okholin, I. N. Verovsky, A. N. Nazarov, V. S. Lysenko, K. I. Kholostov, V. P. Bondarenko, Y. Ishikawa, *Semiconductors* **2011**, *45*, 350.

[267] Y. Ding, H. Shirai, *J. Appl. Phys.* **2009**, *105*, 043515.

[268] Y. Peng, J. Zhou, X. Zheng, B. Zhao, X. Tan, *Int. J. Mod. Phys. B* **2011**, *25*, 2983.

[269] X. Liu, L. Cao, H. Song, H. Jiang, *Physica E* **2014**, *61*, 167.

[270] L. Cao, X. Liu, H. Jiang, H. Song, J. Zhao, H. Lu, *J. Nanosci. Nanotechnol.* **2014**, *14*, 3928.

[271] J. Zhang, S. Yan, Q. Jia, J. Huang, L. Lin, S. Zhang, *Physica E* **2016**, *80*, 19.

[272] J. R. Ramos-Serrano, Y. Matsumoto, C. Morales, in *2018 15th Int. Conf. on Electrical Engineering, Computing Science and Automatic Control (CCE 2018)*, IEEE, Mexico City **2018**, https://doi.org/10.1109/ICEEE.2018.8533970.

[273] A. V. Vasin, Y. Ishikawa, S. P. Kolesnik, A. A. Konchits, V. S. Lysenko, A. N. Nazarov, G. Y. Rudko, *Solid State Sci.* **2009**, *11*, 1833.

[274] I. García, C. Morales, E. Rosendo, T. Díaz, M. Pérez, E. Gastellóu, R. Serrano, R. Galeazzi, G. García, R. Romano, A. Coyopol, R. Portillo, *Thin Solid Films* **2020**, *713*, 138358.

[275] A. V. Vasin, M. Adlung, V. A. Tertykh, D. Kysil, S. Gallis, A. N. Nazarov, V. S. Lysenko, *J. Lumin.* **2017**, *190*, 141.

[276] J. Botsoa, V. Lysenko, A. Géloën, O. Marty, J. M. Bluet, G. Guillot, *Appl. Phys. Lett.* **2008**, *92*, 2006.

[277] Y. Zakharko, T. Serdiuk, T. Nychyporuk, A. Géloën, M. Lemiti, V. Lysenko, *Plasmonics* **2012**, *7*, 725.

[278] F. Erogbogbo, X. Liu, J. L. May, A. Narain, P. Gladding, M. T. Swihart, P. N. Prasad, *Integr. Biol.* **2013**, *5*, 144.

[279] G. Dravecz, T. Z. Jánosi, D. Beke, D. Major, G. Károlyházy, J. Erostyák, K. Kamarás, Á. Gali, *Phys. Chem. Chem. Phys.* **2018**, *20*, 13419.

[280] J.-H. Park, L. Gu, G. von Maltzahn, E. Ruoslahti, S. N. Bhatia, M. J. Sailor, *Nat. Mater.* **2009**, *8*, 331.

[281] N. Singh, A. Karambelkar, L. Gu, K. Lin, J. S. Miller, C. S. Chen, M. J. Sailor, S. N. Bhatia, *J. Am. Chem. Soc.* **2011**, *133*, 19582.

[282] R. Intartaglia, K. Bagga, M. Scotto, A. Diaspro, F. Brandi, *Opt. Mater. Express* **2012**, *2*, 510.

[283] E. Borsella, R. D'Amato, M. Falconieri, E. Trave, A. Panariti, I. Rivolta, *J. Mater. Res.* **2013**, *28*, 193.

[284] E. Marin, T. Adachi, M. Zanocco, F. Boschetto, A. Rondinella, W. Zhu, S. Somekawa, R. Ashida, R. M. Bock, B. J. McEntire, B. S. Bal, O. Mazda, G. Pezzotti, *Mater. Sci. Eng., C* **2020**, *106*, 110278.

[285] J. Morales-Chávez, J. Herrera-Celis, Z. Saldana-Ahuactzi, C. Reyes-Betanzo, F. J. Gómez-Montaño, A. Orduña-Díaz, *Surf. Interfaces* **2020**, *20*, 100550.

[286] F. J. Gómez-Montaño, A. Orduña-Díaz, *Anal. Lett.* **2021**, *54*, 2655.

[287] R. R. Hu, Z. Z. Yin, Y. B. Zeng, J. Zhang, H. Q. Liu, Y. Shao, S. Bin Ren, L. Li, *Biosens. Bioelectron.* **2016**, *78*, 31.

[288] D. Jiang, P. Zhu, H. Jiang, J. Ji, X. Sun, W. Gu, G. Zhang, *Biosens. Bioelectron.* **2015**, *70*, 482.

[289] D. Harpaz, B. Koh, R. C. S. Seet, I. Abdulhalim, A. I. Y. Tok, *Talanta* **2020**, *212*, 120792.

[290] M. Antoniou, D. Tsounidi, P. S. Petrou, K. G. Beltsios, S. E. Kakabakos, *Med. Devices Sens.* **2020**, *3*, e10072.

[291] M. J. Bañuls, V. González-Pedro, C. A. Barrios, R. Puchades, Á. Maquieira, *Biosens. Bioelectron.* **2010**, *25*, 1460.

[292] B. L. Gilmore, J. R. Tanner, A. O. McKell, C. E. Boudreaux, M. J. Dukes, S. M. McDonald, D. F. Kelly, *Micromachines* **2013**, *4*, 90.

[293] F. Boschetto, T. Adachi, S. Horiguchi, D. Fainozzi, *J. Biomed. Opt.* **2018**, *23*, 056002.

Ateet Dutt is the leader of the nanomaterials growth laboratory (https://www.iim.unam.mx/maver/de-nano/) at the Materials Research Institute, National Autonomous University of Mexico (IIM-UNAM). He received a Ph.D. from CINVESTAV, Mexico, in 2015 and is a member of the System of National Researchers (CONACyT). He has published several articles in reputed international peer-review journals, holds a Mexican patent, and has delivered invited talks at different conferences. He is also on the editorial board of several leading nanotechnology journals. His primary research is focused on developing silicon nanoparticles, zinc oxide nanowires, and MoOx thin films for various optoelectronic applications like the potential development of LEDs, third-generation solar cells, catalysis (hydrogen production), and sensors, among others.

Rafael Salinas is a postdoctoral fellow at the Universidad Nacional Autónoma de México (UNAM, México). He received a Ph.D. in applied biotechnology from Instituto Politécnico Nacional (CIBA-IPN). He has published nine research articles, two proceedings, and two patent applications. His current interest relies on developing biofunctionalization strategies for pathogen detection based on the attachment of different biological recognition molecules on thin-film transistors, ZnO platforms, and semiconductor materials to potentiate their applications in the biological field.

Shirlley Martínez Tolibia obtained a Ph.D. in applied biotechnology from Instituto Politécnico Nacional (CIBA-IPN). She received her bachelor's degree in chemical engineering from Benemérita Universidad Autónoma de Puebla. Her research interest is based on bacterial genetics, bioprocess development, dielectric spectroscopy for cell differentiation monitoring, and molecular validations of transcriptional control and protein expression. Additionally, she is interested in applying biological molecules to recognize pathogenic agents of different types.

Ebrahim Mostafavi has so far received training at Stanford University School of Medicine (PostDoc), Northeastern University (Ph.D.), Harvard Medical School (Researcher), and University of Tehran (M.Sc. and B.Sc.). His research interests revolve around the engineering and development of (nano) biomaterials, nanocarriers, and 3D in vitro models (hydrogels, 3D bioprinted constructs, nanofibrous scaffolds, organoids, vascular grafts, and microfluidic systems) to create biologically complex systems for a range of applications such as tissue engineering and regenerative medicine, translational medicine, cancer therapy (with focus on women's cancer), biosensing, and infectious diseases. He serves as associate editor-in-chief of several prestigious and high-impact journals within Elsevier, Springer, Cell Press, Dove Medical Press, T&F, Frontiers, etc.

Yogendra Kumar Mishra is professor MSO and Leader of Smart Materials group at Mads Clausen Institute, University of Southern Denmark (SDU), Sønderborg, Denmark. Previously, he was leading an independent research group on 3D nanomaterials at Functional Nanomaterials Chair, Kiel University. The Smart Materials group's main focus is to develop new class of 'Smart Materials for Advanced and Sustainable Technologies'. He is editorial board member and referee for many prestigious magazines. He has received many notable awards, like, Alexander von Humboldt fellowship (2008), Young Investigator Award (under 40) from BHJ Fonden-Denmark, and has won several successful grants.

Yasuhiro Matsumoto is a full-time professor at Electrical Engineering Department, CINVESTAV, Mexico City. The doctorate degree was conferred from the Faculty of Engineering Science, Osaka University, Japan, in 1990. Since 1985, he has been a research associate at CINVESTAV, mainly in the field of crystalline silicon solar cell production. From 1991, he worked in plasma CVD-deposited amorphous silicon carbide; silicon oxide; silicon nitride; and their application to a-Si thin film devices such as TFT and solar cells. Since 2002, he has dedicated himself to catalytical chemical vapor deposition (Cat-CVD) for silicon oxide and, lately, SiO_xC_y-related nanocrystalline materials using organic-based sources such as TEOS and MMS mostly for photoluminescence.

Guillermo Santana Rodríguez began to work in the Department of Condensed Materials at the Institute of Materials and Reagents of the University of Havana (IMRE) as a technological researcher. He specialized in photolithography processes to manufacture different detectors, such as CCD and point position markers. He worked on different silicon solar cell technologies, for example, buried contact solar cells and electroless nickel contacts solar cells (1986–1989). His research involved selective emitter solar cells and silicon nitride films as a passivating and antireflective coating for silicon solar cells. To date, he belongs to the National System Researchers in maximum level (Level 3), has to his credit more than 140 extensive publications, four published books, and more than 200 papers presented at different conferences and symposia.

Ajeet Kaushik, fellow ICS, is working as an assistant professor of Chemistry at Florida Polytechnic University, USA, and exploring nanoenabled technology for health wellness, involving efficient sensing and nanomedicine. He is an accomplished scholar (supported by his publications, editorial roles, edited books, patents, and international collaborations) and the recipient of several international awards supporting his credentials. His research interests include green chemistry, electrochemistry, chemical sensors, biosensors, nanomedicine, point-of-care sensing, and personalized sensing. To achieve goals, he is focused on cutting-edge research and seeking collaborations.